Optimal 6E design of an integrated solar energy-driven polygeneration and CO₂ capture system: A machine learning approach

Nastaran Khani [a], Mohammad H. Khoshgoftar Manesh [a], Viviani C. Onishi [b],[*]

[a] *Energy, Environmental and Biological Systems Research Lab (EEBRlab), Division of Thermal Sciences and Energy Systems, Department of Mechanical Engineering, Faculty of Technology & Engineering, University of Qom, Qom, Iran*

[b] *School of Computing, Engineering and the Built Environment, Edinburgh Napier University, Merchiston Campus, 10 Colinton Road, Edinburgh EH10 5DT, UK*

A B S T R A C T

Renewable energy-driven decentralized polygeneration systems herald great potential in tackling climate change issues and promoting sustainable development. In this light, this study introduces a new machine learning-based multi-objective optimization approach of an integrated solar energy-driven polygeneration and CO₂ capture system for meeting a greenhouse's power, freshwater, and CO₂ demands. The integrated solar-assisted polygeneration system comprises a 486-kW gas turbine, two steam turbines, two organic Rankine cycles, a humidification-dehumidification desalination unit to recover waste heat while producing freshwater, and a post-combustion CO₂ capture unit. The proposed system is mathematically modelled and evaluated via a dynamic simulation approach implemented in MATLAB software. Moreover, sensitivity analysis is conducted to identify the most influential decision variables on the system performance. The machine learning-based multi-objective optimization strategy combines Genetic Programming (GP) and Artificial Neural Networks (ANN) to minimize total costs, environmental impacts, and economic and environmental emergy rates whilst maximizing the system exergy efficiency and freshwater production. Finally, the system performance is further investigated through comprehensive Energy, Exergy, Exergoeconomic, Exergoenvironmental, Emergoeconomic, and Emergoenvironmental (6E) analyses. The three-objective optimization of the integrated system reduces total costs, environmental impacts, and monthly environmental emergy rate by 11.4%, 34.31% and 6.38%, respectively. Furthermore, reductions up to 56.81%, 50.19% and 77.07%, respectively, are obtained for the previous indicators by the four-objective optimization model. Hence, the proposed multi-objective optimization methodology represents a valuable tool for decision-makers in implementing more cost-effective and environment-friendly solar-assisted integrated polygeneration and CO₂ capture systems.

Introduction

Sustainable decentralized polygeneration of power, heating, cooling, and freshwater, among other products, has become an exceedingly attractive field of study throughout the last decades due to ever-growing energy demands and water scarcity. In this framework, the combination of solar thermal energy with polygeneration and desalination plants has gained attention worldwide, particularly in water-stressed countries with high solar energy potential including the United States, China, India, Australia, northern and western Africa [1,2]. The integrated design and optimization of renewable energy-based polygeneration plants can lead to improved overall system efficiencies and, consequently, important energy, costs, and environmental savings due to the optimal integration of the different subsystems and equipment sharing [3]. Yet, the optimal design of solar-assisted polygeneration systems integrated with desalination processes and other relevant subsystems is a challenging task, usually requiring advanced thermodynamic, economic, and environmental-based analysis and computer-aided tools.

The literature highlights the significance of solar thermal energy integration with trigeneration and polygeneration systems to enhance energy efficiency and sustainability. In this way, Dabwan et al. [4] have studied an integrated gas turbine-based trigeneration plant with parabolic-trough collectors (PTC) for producing power, cooling, and freshwater. The results from their thermo-economic analysis of the integrated system show that the levelized electricity cost increases when PTC is coupled to the gas turbine cycle. At the same time, carbon emissions are reduced by 385k tons/year. El-Emam and Dincer [5] have

Nomenclature

Roman letters

a	Specific area (m^2/m^3)
A	Area (m^2)
b	Environmental impact per exergy unit (mPts/kJ)
$\dot{B}$	Environmental impact rate (mPts/s)
b_m	Environmental impact per mass unit
C	Cost per exergy unit (US\$/kJ)
$\dot{C}$	Cost rate (US\$/s)
$Cond$	Condenser
C_p	Specific heat at constant pressure (kJ/kg.K)
EL	Electricity consumption of CO_2 capture (kJ)
$\dot{Ex}$	Exergy rate (kJ/s)
f	Exergoeconomic factor
f_b	Exergoenvironmental factor
f_m	Emergy-based exergoeconomic factor
f_n	Emergy-based exergoenvironmental factor
G	Mass flowrate of air per area in HDH (kg/s.m^2)
h	Specific enthalpy (kJ/kg)
h_g	Convective heat transfer coefficient (W/m^2. °C)
k_g	Mass transfer coefficient of air/water mixture (kg/s.m^2)
L	Mass flowrate of water per area in HDH (kg/s m^2)
m	Specific economic emergy (sej/J)
$\dot{m}$	Mass flowrate (kg/s)
$\dot{M}$	Economic emergy rate (sej/s or sej/h)
n	Specific environmental emergy (sej/J)
$\dot{N}$	Environmental emergy rate (sej/s or sej/h)
n_{mirror}	Number of mirrors
P	Pressure (kPa)
r	Relative cost difference
r_m	Relative economic emergy difference
r_n	Relative difference of environmental emergy
r_p	Pressure ratio
T	Temperature (K)
TIP	Turbine inlet pressure (K)
TIT	Turbine inlet temperature (K)
$\dot{U}$	Component-related economic emergy rate (sej/s or sej/h)
$\dot{V}$	Component-related environmental emergy rate (sej/s or sej/h)
W	Work (kJ)
x	Mole fraction
X	Packing length (m)
y	Environmental impact of the component (mPts)
Y	Packing width (m)
$\dot{Y}$	Environmental impact rate of the equipment (mPts/s)
$\dot{Z}$	Cost rate of the equipment (US\$/s)

Subscripts:

0	Ambient condition
c	Collector
d	Dehumidifier
D	Destruction
F	Fuel
fg	Flue gas
g	Gas-phase (air/water mixture)
h	Humidifier
i	Interface
k	Counter of components

P	Product
q	Heat
th	Therminol
s	Steam
sub	Subcritical
u	Useful
w	Work
wb	Water bulb

Acronyms:

AC	Air Compressor
ANN	Artificial Neural Network
ARC	Absorption Refrigeration Cycle
CC	Combustion Chamber
CCS	Carbon Capture and Storage
CCHP	Combined Cooling, Heat and Power
Cond	Condenser
DHW	Domestic Hot Water
DNI	Direct Normal Irradiance
DV	Decision Variable
ECO	Economizer
EVA	Evaporator
GP	Genetic Programming
GT	Gas Turbine
GWP	Global Warming Potential
HDH	Humidification-Dehumidification
HPP	High-Pressure Pump
HRSG	Heat Recovery Steam Generator
HX	Heat Exchanger
LCA	Life Cycle Assessment
MOGA	Multi-Objective Genetic Algorithm
MED	Multi-Effect Distillation
MSF	Multi-Stage Flash
MVC	Mechanical Vapor Compression
NGCC	Natural Gas Combined Cycle
OF	Objective Function
ORC	Organic Rankine Cycle
ORCP	Organic Rankine Cycle Pump
ORCT	Organic Rankine Cycle Turbine
PCCC	Post-Combustion Carbon Capture
PTC	Parabolic-Trough Collectors
RO	Reverse Osmosis
S-CO_2	Supercritical Carbon Dioxide
SF	Solar Fraction
SFHX	Solar Field Heat Exchanger
SFP	Solar Field Pump
SPECO	Specific Exergy Costing
ST	Steam Turbine
SUP	Superheater

Greek letters:

γ	Ratio of the specific heats
λ_0	Latent heat of vaporization
ΔT	Temperature difference
ΔP	Pressure difference
ε	Exergy efficiency
η	Efficiency
ν	Specific volume
ω	Humidity ratio

proposed a polygeneration system integrating solar heliostat energy, steam turbine, absorption cooling system and seawater RO desalination unit. The authors evaluated the energy and exergy efficiencies of the polygeneration system for producing power, heating and cooling, freshwater, and hydrogen. Ghorbani et al. [6] have performed energy, exergy, and economic analyses of a solar-assisted polygeneration system to produce power and liquid fuels. Their results indicate total energy and exergy efficiencies of 42.36% and 64.72%, respectively. Ghorbani et al. [7] have performed energy and exergy analyses of a solar-assisted tri-generation system composed of solar parabolic dish collectors. Their proposed cycle generates 4.36 MW power, 2026 kg/h hydrogen, and 1.65 MW cooling. The overall system energy and exergy efficiencies are reported at 90.77% and 92.19%, respectively.

The combination of solar energy with other renewable resources in so-called hybrid polygeneration systems has also been explored in the pertaining literature. Mouaky and Rachek [8] have conducted the thermo-economic analysis of a hybrid solar-biomass polygeneration system located in the semi-arid region of Benguerir, Morocco. Their proposed hybrid configuration generates 0.231 €/kWh electricity, 0.86 €/m^3 freshwater, and 0.047 €/kWh domestic hot water (DHW) by the aid of solar and biomass. Their thermo-economic analysis indicates an increase in energy efficiency from 11.35 to 16.32%, while the exergy efficiency is improved from 5.33 to 5.96%. Tukenmez et al. [9] have developed a solar-biomass polygeneration system for producing power, hydrogen and ammonia. The proposed integrated system encompasses a concentrating solar power plant composed of parabolic dish collectors. The results from energy and exergy system analyses reveal 58.76% energy and 55.64% exergy efficiencies, whereas the total electrical energy output is rated at approximately 20 MW.

Solar-assisted thermal desalination has emerged as a promising technology for mitigating greenhouse gas emissions and overcoming the freshwater shortages in recent years. Among thermal desalination technologies such as reverse osmosis (RO), multi-stage flash (MSF), multi-effect distillation (MED) and mechanical vapor compression (MVC), RO and MED are the most prevalent methods in large-scale industrial plants. However, humidification-dehumidification (HDH) technology is suitable for low-scale building applications due to its simple structure, low operating costs, easy control, high efficiency, and the possibility of using inexpensive low-grade heat sources [10]. For these reasons, several authors have studied the thermodynamic efficiency and economic and environmental aspects of solar-assisted HDH desalination systems. Deniz and Çinar [11] have performed an energy, exergy, economic and environmental analyses of the HDH process. The highest value of the daily energy efficiency and the maximum exergy efficiency are reported at 31.54% and 1.87%, respectively. Zubair et al. [12] have evaluated the performance and costs of a HDH desalination system coupled with a solar evacuated tube collectors. Their results show that the amount of freshwater generated varies from 16,430 to 19,445 L with prices ranging from 0.032 to 0.038 US$ per liter for distinct locations. Recent studies have also investigated the integration of HDH desalination with polygeneration systems. Ghiasirad et al. [13] have conducted a thermo-economic evaluation of a combined power, heating and cooling system with HDH desalination. Their results demonstrate energy and exergy efficiencies of 70.58% and 43.59%, respectively for winter, and 60.55% and 17.05%, respectively for the summer season.

Based on the Intergovernmental Panel on Climate Change (IPCC) recommendations, a 50–80% reduction in carbon dioxide emissions is necessary by the year 2050 [14]. Therefore, in addition to combining renewable energy resources, integrating CO_2 capture technologies into polygeneration systems and combined power plants can also be beneficial in cutting down carbon emissions and achieving those recommendations. Patiño and Rivera [15] have carried out a thorough analysis of net power output and global warming potential (GWP) of an integrated natural gas combined cycle (NGCC) power plant with organic Rankine cycles (ORCs) and post-combustion carbon capture (PCCC).

Their results indicate that the decrease in CO_2 emissions reduce GWP by 78%. Liu et al. [16] have used energy, exergy, economic and environmental analyses to evaluate an integrated system configuration consisting of carbon capture and storage (CCS), ORC, and an absorption refrigeration cycle (ARC) using waste heat as heat source. The authors obtained an exergy efficiency of 42.88%, while the total annual cost was 72% lower than the basic CCS system. Botero et al. [17] have considered a 400-MW NGCC integrated with post-combustion CO_2 capture. Their study combines redesign, optimization, and economic evaluation of the proposed integrated system. The authors reported that employing PCCC increases capital costs by 43% compared to the plant without the CO_2 capture unit. Nevertheless, the costs were decreased by about 20–30% in the CO_2 capture section.

Developing appropriate design and optimization tools to simultaneously reduce energy utilization, costs and environmental impacts is one of the major challenges in polygeneration systems. Nowadays, there is a growing interest in energy industry and academia in the application of advanced energy, exergy, exergoeconomic, exergoenvironmental, emergoeconomic, and emergoenvironmental analyses –varying from 3E to 6E analyses –to achieve bettered solutions. Khoshgoftar Manesh et al. [18] have applied exergy, exergoeconomic, and exergoenvironmental (3E) analyses of a combined power plant consisting of a gas turbine (GT) power cycle, supercritical carbon dioxide (S-CO_2) cycle, ORC, and RO desalination unit. The authors reported that the integration of S-CO_2 and GT cycles boosts the total efficiency by 10.9%. Khoshgoftar Manesh et al. [19] have investigated the redesign of Neka's combined cycle power plant in Iran by integrating a RO-MED desalination system using conventional and advanced 3E analyses. Their results indicate an exergy efficiency of 42.7% for the integrated power and desalination system.

Jadidi et al. [20] have conducted conventional and advanced energy, exergy, exergoeconomic, and exergoenvironmental (4E) analyses of a solar-assisted cogeneration system comprised by PTC, integrated gasification combined power cycle, and CO_2 absorber technology. Their results show system energy and exergy efficiencies of 50% and 54%, respectively. Anvari et al. [21] have implemented 4E analyses to assess a multigeneration system for producing power, heating and cooling, and desalinated water. Their results reveal total costs 1943.5 US$/h and total CO_2 emissions of 0.163 kg/kWh. They also suggested that increasing of the pre-heater outlet temperature yields to a reduction of 26% in the system CO_2 emissions.

Ehyaei et al. [22] have performed energy, exergy, economic, exergoenvironmental, and environmental (5E) analyses of a geothermal-driven polygeneration system integrated with RO desalination and electrolysis. The proposed system generates around 1.8 GJ/year electricity, 18k m^3/year freshwater, 1.04 GJ/year cooling energy, 3.838 ton/year sodium-hypochlorite, and 7.396 ton/year hydrogen. Their results indicate energy and exergy efficiencies of 12.25% and 19.6%, respectively. Nourpour and Khoshgoftar Manesh [23] have studied the energy, exergy, exergoeconomic, exergoenvironmental, emergoeconomic, and emergoenvironmental (6E) analyses of a quadruple combined power cycle. The proposed system integrates steam and ORCs for promoting waste heat recovery and boosting power generation. Their results indicate that cycle energy efficiency is increased by 16% compared to GTs. Khani et al. [3] have conducted a comprehensive 6E analyses of a solar energy-driven polygeneration system integrating ORCs, post combustion CO_2 capture, and HDH desalination. Their results show an increase of 37.3% in power generation due to the solar energy integration.

In the framework of optimization approaches, Makkeh et al. [24] have developed an energy, exergy, and exergoeconomic approach for the optimal design of a cogeneration system integrated with desalination, wind and solar thermal energy generation. Their system is aimed at supplying the power and freshwater requirements in Iran by integrating PTC, wind turbines, ORC, and RO, MED, and thermal vapor compression desalination systems. Their results show that the proposed approach reduces the water production cost by 23%. Moreover, results from multi-
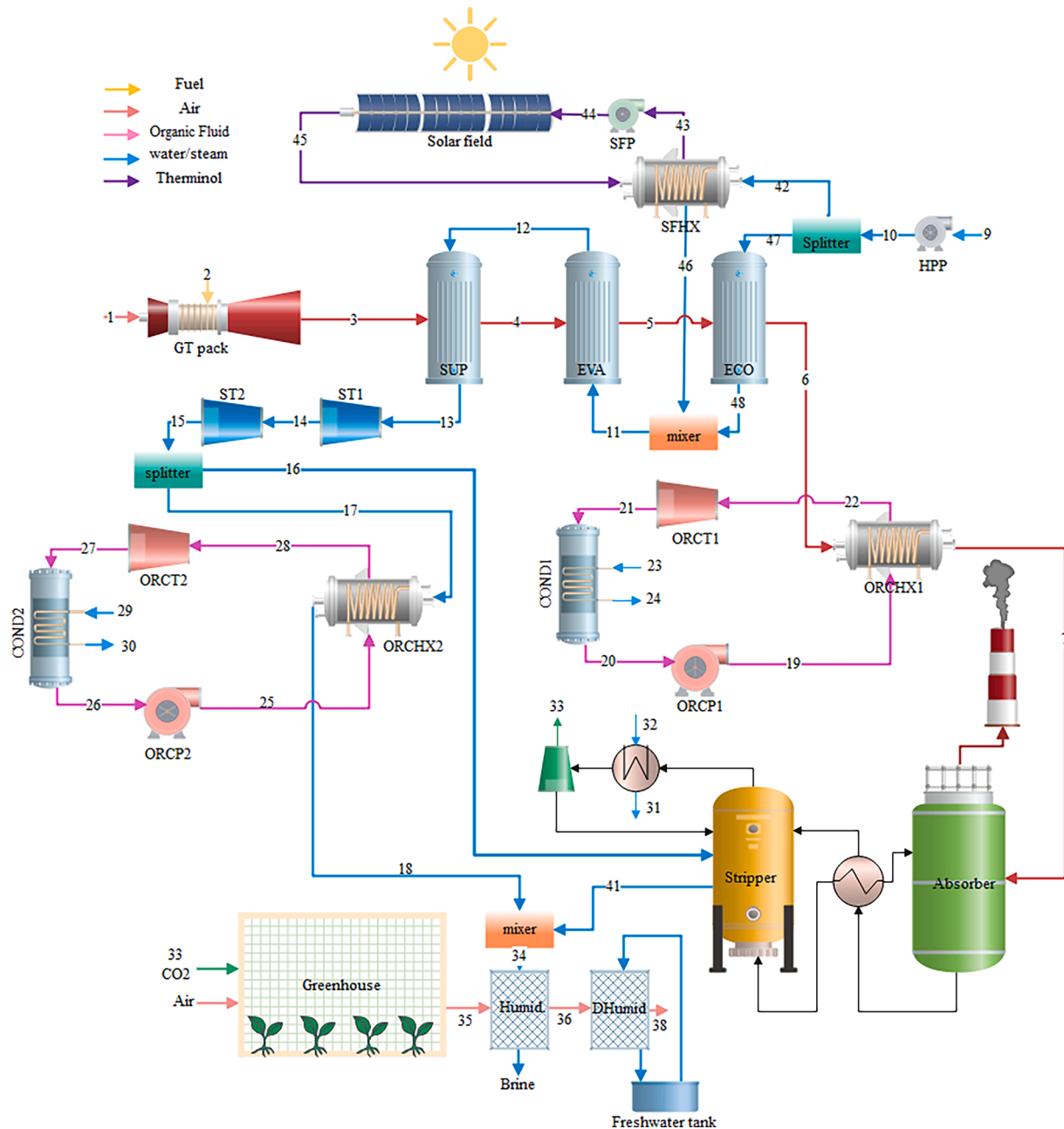
Fig. 1. Schematic diagram of the proposed integrated solar energy-driven polygeneration and CO_2 capture system (adapted from Khani et al., [3]).

objective optimization indicate exergy efficiency and freshwater production cost of 26.2% and 3.08 US$/m^3, respectively. The methodology led to an optimal design in which the annual CO_2 emissions are reduced by 52,164 tons/year.

Abbasi and Pourrahmani [25] have presented an optimization approach to improve the exergoeconomic performance of a hydrogen and freshwater cogeneration system integrated with HDH desalination. To find optimal solutions, the authors have performed single and multi-objective system optimizations. The system exergy efficiency, freshwater and hydrogen costs are reported at 22.49%, 2.94 US$/m^3, and 7.37 US$/kg, respectively. Liu et al. [26] have proposed an exergoeconomic analysis and multi-objective optimization approach using NSGA-II to determine the optimal design parameters of a combined cooling, heat and power (CCHP) system with CO_2 capture. The authors assumed as decision variables for the optimal design the outlet pressures of the liquefied natural gas pump and multistage compressor, CO_2 flowrate in the district cooling cycle, and isentropic efficiencies of

turbines. Their results suggest that the total energy output, exergy efficiency, and cost per unit exergy are improved significantly by the optimization method.

The previous literature review indicates that there is currently a lack of studies on the simultaneous application of 6E analyses and machine learning-based multi-objective optimization of decentralized, integrated solar energy-driven polygeneration and CO_2 systems. To address shortcomings in preceding research, this study introduces a new comprehensive approach for the optimal design of integrated solar-assisted polygeneration and CO_2 capture systems for sustainable power, freshwater and CO_2 production in greenhouse applications. The proposed polygeneration system integrates gas and steam turbine power cycles, ORCs, HDH desalination, post-combustion CO_2 capture, and a solar energy field composed of parabolic-trough collectors. A dynamic simulation model is implemented in MATLAB software to determine the system operating conditions, and the results are verified against literature data and simulations via THERMOFLEX software. Moreover, a solar

Table 1

Exergy analysis relationships used to model different system equipment units.

Definition	Exergy Equation	Ref.
Steady-state exergy balance	$\sum \dot{Ex}_{in} - \sum \dot{Ex}_{out} - \dot{Ex}_D = 0$	[28]
Physical specific exergy	$ex_{Ph} = (h - h_0) - T_0(s - s_0)$	[28]
Chemical specific exergy	$ex_{Ch} = \sum x_k e\overline{x}_k{}^{CH} + \overline{R}T_0 \sum x_k \ln(x_k)$	[28]
Overall exergy	$ex_K = ex_{Ch} + ex_{ph}$	[28]
Exergy efficiency	$\varepsilon_{ex} = \dfrac{\dot{Ex}_P}{\dot{Ex}_F} = 1 - \dfrac{\dot{Ex}_D}{\dot{Ex}_F}$	[28]
Rate of the exergy destruction	$\dot{Ex}_D = \dot{Ex}_F - \dot{Ex}_P$	[28]
Solar field exergy	$\dot{Ex}_{solar} = \dot{Q}_{solar}\left(1 - \dfrac{4}{3}\dfrac{T_a}{T_{sun}}\left(1 - 0.28\ln f_{dil}\right)\right)$	[29]
Humid air exergy	$ex_{da} = (c_{p,a} + \omega c_{p,v})T_0(\dfrac{T}{T_0} - 1 - \ln\dfrac{T}{T_0}) +$ $(1 + 1.608\omega)R_a T_0 \ln\dfrac{P}{P_0} +$ $R_a T_0(1 + 1.608\omega)\ln\dfrac{1 + 1.608\omega_0}{1 + 1.608\omega} + 1 +$ $1.608\omega\ln\dfrac{\omega}{\omega_0}$	[30]

fraction strategy is adopted to accurately control the steam generation assisted by the solar energy collectors. Sensitivity analysis is performed to identify the most influential decision variables on the system performance, which are then defined as objective functions for system optimizations. A multi-objective genetic algorithm (MOGA) optimization strategy combining Genetic Programming (GP) and Artificial Neural Networks (ANN) is developed to minimize total costs, environmental impacts, and economic and environmental emergy rates while maximizing the system exergy efficiency and freshwater production. Finally, the thermodynamic, economic, and environmental performances of the proposed solar-assisted polygeneration system are further investigated through 6E analyses.

System description

A schematic diagram of the proposed integrated solar energy-driven polygeneration and CO_2 capture system is depicted in Fig. 1. The proposed polygeneration system is based on the authors' previous study presented in Khani et al. [3]. The integrated polygeneration system is composed of a 486-kW gas turbine pack (GT-pack), two steam turbine (ST) cycles, a heat recovery steam generator (HRSG), a post-combustion CO_2 capture unit, and two organic Rankine cycles (ORCs). In addition, a humidification-dehumidification (HDH) desalination unit is employed to recover waste heat from the power cycles while producing freshwater. Furthermore, parabolic Euro trough collectors are utilized as an auxiliary energy system operating in parallel with the economizer to provide heat requirements from solar energy. The specification parameters used to model the solar ET-100 parabolic-trough collectors are presented in Table A.1 of **Appendix A**. The operating performance of the developed polygeneration and CO_2 capture system is briefly described as follows.

The pressurized air from the air compressor (AC) is mixed with fuel (natural gas) combusted in the combustion chamber (CC) to provide the suitable temperature and pressure of the GT-pack. Afterwards, the high-pressure and temperature mixture is expanded through the GT to generate power. Discharged gases from the GT-pack (state 3) are send to the HRSG, consisting of superheater, evaporator, and economizer, to produce additional power via STs by the aid of the solar parabolic-trough collectors. The feed water (state 9) passes through a high-pressure pump and splits according to the average monthly weather data of Qom city. In this way, the higher the average monthly Direct Normal Irradiance (DNI) is, the higher mass flow rate (state 42) enters to the solar field heat exchanger as heat sink. In the solar energy field, Therminol-VP1 is used as heat transfer fluid due to its high thermal

resistance. The heat transfer fluid absorbs solar energy and transfers it to the water. The rest of the water stream (state 47) is heated by the flue gases heat transfer in the economizer. After the heat transfer between the water stream and the fluid Therminol-VP1, the heated-up water stream (state 46) is mixed with the outlet water from the economizer. Then, the mixture is fed into the evaporator before entering the super-heater to reach a high degree of steam and meet the inlet STs requirements.

In the proposed integrated polygeneration and CO_2 capture system, additional power is generated by implementing two ORCs after the economizer and ST cycles. This configuration improves the energy performance of the system by taking advantage of the waste heat from exhausted gases and steam which serve as heat sources for the ORCs. Before the flue gases are discharged into the atmosphere (state 7), CO_2 is captured in a post-combustion carbon capture (PCCC) unit to make the cycle eco-friendly and provide the required CO_2 concentration for the greenhouse. The water-steam mixture of streams (state 41) and (state 18) is used to supply the inlet hot water of the HDH desalination unit and generate freshwater. In the HDH unit, direct contact open-air, open water humidifier and dehumidifier units with packing bed structure are employed to increase the contact surface area between water and air. Thus, heat and mass transfer between the sprayed hot water (state 34) and the air from the greenhouse (state 35) boost temperature and humidity of the air stream. In the dehumidifier, the inlet humid air stream (state 36) is cooled and condensed, and cold freshwater (state 40) is heated as a result of difference in the air/water interface humidity ratio. Finally, freshwater is generated and stored in freshwater tank to be used according to the greenhouse demands.

System modelling approach

Energy analysis

The thermodynamic analysis is performed via energy and mass conservation balances to determine the optimal operating conditions of all process streams of the integrated polygeneration system. Table A.2 (see **Appendix A**) presents the thermodynamic relationships used to model the different equipment units, as well as the corresponding assumed inlet conditions (modelling parameters) and estimated outlet conditions (modelling variables). The integrated solar energy-driven polygeneration and CO_2 capture system is mathematically modelled and dynamically simulated in MATLAB software and the results are validated via THERMOFLEX software. Moreover, a solar fraction strategy is adopted to model the parabolic-trough solar collectors with increased accuracy. It should be noted that the solar fraction gives the ratio of the useful gained energy by the solar system to the sum of the same amount and the heat transfer rate of the HRSG. Therefore, this parameter determines the amount of the required heating supplied by the solar section and the one by the HRSG. By increasing the solar fraction, the input flowrate to the solar system will also increase. Furthermore, the governing relations of the CO_2 capture unit are correlated by combining Artificial Neural Network (ANN) and Genetic Programming (GP). Sensitivity analysis is performed to identify the most influential decision variables on the integrated system performance. The resulting multi-objective genetic algorithm (MOGA) modelling approach is implemented in MATLAB software, where the carbon capture unit efficiency, η_{CO_2}, is assumed at 90%.

To simplify the mathematical model formulation, the following assumptions are required:

i. Steady-state and steady flow conditions are assumed in equipment units.
ii. Pure methane is utilized fuel for injection to the combustion chamber.
iii. Negligible changes in potential and kinetic energy and exergy.
iv. Air and flue gas behavior are based on ideal gas laws.

Table 2

Exergoeconomic governing equations.

Definition	Exergoeconomic Equation	Ref.
Cost balance	$\sum_i^N \left(c_i \dot{E}_i \right)_k + c_{q.k} \dot{E}_{q.k} + \dot{Z}_k =$ $\sum_e^N \left(c_e \dot{E}_e \right)_k + c_{w.k} \dot{W}_{q.k}$	[28]
Total cost rate	$\dot{Z}_k = \dfrac{\Phi_k \times PEC_k \times CRF}{3600 \times N}$	[28]
Capital recovery factor	$CRF = \dfrac{i(i+1)^n}{(i+1)^n - 1}$	[28]
Cost rate for exergy destruction	$\dot{C}_{D.k} = c_{F.k} \dot{E}_{D.k}$	[31]
Average cost of fuel per unit exergy	$c_{f.k} = \dfrac{\dot{C}_{F.k}}{\dot{Ex}_{F.k}}$	[31]
Average cost of product per unit exergy	$c_{p.k} = \dfrac{\dot{C}_{P.k}}{\dot{Ex}_{P.k}}$	[31]
Relative cost difference	$r_k = (c_{P.k} - c_{F.k})/c_{P.k}$	[31]
Exergoeconomic factor	$f_k = \dot{Z}_k / \left(\dot{Z}_k + \dot{C}_{D.k} \right)$	[31]

Table 3

Exergoenvironmental governing equations.

Definition	Exergoenvironmental Equation	Ref.
Environmental impact balance	$\sum_i^N \left(b_i \dot{E}_i \right)_k + b_{q.k} \dot{E}_{q.k} + \dot{Y}_k =$ $\sum_e^N \left(b_e \dot{E}_e \right)_k + b_{w.k} \dot{W}_{q.k}$	[34]
Environmental impact rate	$\dot{Y}_k = \dfrac{Y_k}{3600 Nn}$	[34]
Environmental impact per exergy unit	$b_{f.k} = \dfrac{\dot{B}_{F.k}}{\dot{Ex}_{F.k}}$	[34]
Environmental impact per exergy unit	$b_{p.k} = \dfrac{\dot{B}_{P.k}}{\dot{Ex}_{P.k}}$	[34]
Environmental impact rate of exergy destruction	$\dot{B}_{D.k} = b_{f.k} \times \dot{E}_{D.k}$	[34]
Relative environmental impacts difference	$r_{b.k} = (b_{p.k} - b_{F.k})/b_{P.k}$	[34]
Exergoenvironmental factor	$f_{b.k} = \dot{Y}_k / \left(\dot{Y}_k + \dot{B}_{D.k} \right)$	[34]

Table 4

Emergoeconomic governing equations [35].

Definition	Emergoeconomic Equation
Emergy cost balance	$\sum_i^N \left(m_i \dot{E}_i \right)_k + m_{q.k} \dot{E}_{q.k} + \dot{U}_k =$ $\sum_e^N \left(m_e \dot{E}_e \right)_k + m_{w.k} \dot{W}_{q.k}$
Component-related economic emergoeconomic	$\dot{U}_k = \dot{U}_k^{CI} + \dot{U}_k^{OM}$
Economic emergy rate associated with exergy destruction	$\dot{M}_{D.k} = m_{F.k} \dot{E}_{D.k}$
Total economic emergy rate	$\dot{M}_{TOT.k} = \dot{M}_{D.k} + \dot{U}_k$
Specific emergoeconomic values for fuel	$m_{F.k} = \dfrac{\dot{M}_{F.k}}{\dot{E}_{F.k}}$
Specific emergoeconomic values for product	$m_{P.k} = \dfrac{\dot{M}_{P.k}}{\dot{E}_{P.k}}$
Relative emergy-based cost difference	$r_{m.k} = (m_{p.k} - m_{F.k})/m_{p.k}$
Emergy-based exergoeconomic factor	$f_{m.k} = \dot{U}_k / \left(\dot{U}_k + \dot{M}_{D.k} \right)$

   v. Euro Trough ET-100 solar collectors with Therminol-VP1 as the heat transfer fluid are used in the solar energy field.

   vi. A packed bed crossflow HDH unit is considered for freshwater production.

   vii. Post-combustion CO_2 capture technology is implemented for carbon capture.

Exergy analysis

Exergy analysis is a powerful tool to determine irreversibilities and inefficiencies of integrated power cycles. The main equations used for the exergy analysis of the proposed solar energy-driven polygeneration and CO_2 capture system are exhibited in Table 1. The rate of exergy destruction, as shown in Table 1, indicates the exergy difference between fuel and product in each system component. The exergy analysis is conducted by using the fuel-product-loss (F-P-L) definition proposed by Lozano and Valero [27]. Fuel exergy is defined as the input exergy that converts to the product exergy, which is the main objective of an equipment unit. Hence, the exergy degradation of a sub-system or equipment unit can be explained as losses of the fuel exergy or exergy loss of the system. The exergy destruction occurs when a unit transforms resources into products.

Exergoeconomic analysis

In this study, exergoeconomic analysis is performed to better understand the strengths and weaknesses in terms of irreversibilities and costs of the devised solar-assisted polygeneration and CO_2 capture system. By combining exergy and economic assessments, the exergoeconomic analysis provides more information about the system performance that is not attainable by simply applying thermodynamic or exergy analyses. In addition, the exergoeconomic analysis estimates the cost rate of exergy destruction, products, and fuels. The exergoeconomic governing equations are listed in Table 2.

In Table 2, the cost balance relation for different system equipment units is grounded on the Specific Exergy Costing (SPECO) method proposed in Ref. [32]. Moreover, in the total cost rate equation, the parameter Φ_k stands for the maintenance factor which is equal to 1.06 [33], N is the number of operating hours per year (8000 h) whilst PEC_k represents the purchasing cost of each system component expressed in dollars as given by the cost equations presented in Table A.3 (see **Appendix A**).

Exergoenvironmental analysis

Exergoenvironmental analysis is conducted to improve the exergy and environmental system performances by reducing system inefficiencies while ensuring the lowest greenhouse gas emissions. In this study, the exergoenvironmental analysis is founded on the combination of exergy analysis and life cycle assessment (LCA). The latter uses Eco-indicator 99 to determine the total environmental impacts of system components as a function of their weight and construction type. Exergoenvironmental governing equations are presented in Table 3, and the weight functions of different equipment units are shown in Table A.4 in **Appendix A**.

Emergy analysis

Emergy combines exergoeconomic and exergoenvironmental analyses to simultaneously evaluate economic and environmental system performances. In this regard, input parameters of the system should be merged into a single unit that is defined as solar equivalent of emergy joules or *sej*. Therefore, in the context of emergy assessment, input parameters must be multiplied by the emergy conversion factor β (~ 0.93) which is estimated by the following equation.

$$\beta = 1 + \frac{1}{3}\left(\frac{T_0}{T_S}\right)^4 - \frac{4}{3}\left(\frac{T_0}{T_S}\right) \tag{1}$$

Where T_0 and T_S express the ambient and sun temperatures, respectively.

Table 5
Emergoenvironmental governing equations [35].

Definition	Emergoenvironmental Equation
Emergy-based exergoenvironmental balance	$\sum_i^N \left(n_i \dot{E}_i \right)_k + n_{q.k} \dot{E}_{q.k} + \dot{V}_k =$ $\sum_e^N \left(n_e \dot{E}_e \right)_k + n_{w.k} \dot{W}_{q.k}$
Environmental emergy rate	$\dot{V}_k = \dot{V}_k^{CO} + \dot{V}_k^{OM} + \dot{V}_k^{DI}$
Environmental impact rate associated with exergy destruction	$\dot{N}_{D.k} = n_{F.k} \dot{E}_{D.k}$
Total environmental emergy rate	$\dot{N}_{TOT.k} = \dot{N}_{D.k} + \dot{V}_k$
Specific emergoenvironmental values for fuel	$n_{F.k} = \dfrac{\dot{N}_{F.k}}{\dot{E}_{F.k}}$
Specific emergoenvironmental values for product	$n_{P.k} = \dfrac{\dot{N}_{P.k}}{\dot{E}_{P.k}}$
Relative environmental emergy difference	$r_{n.k} = (n_{P.k} - n_{F.k})/n_{P.k}$
Emergy-based exergoenvironmental factor	$f_{n.k} = \dfrac{\dot{V}_k}{\left(\dot{V}_k + \dot{N}_{D.k} \right)}$

Emergoeconomic analysis

Emergoeconomic methodology is based on the conventional exergoeconomic evaluation, where the SPECO methodology [32] is applied to each stream of the proposed integrated system. The emergoeconomic analysis formulation is summarized in Table 4.

In Table 4, $\dot{U}_k$ is defined as the sum of capital investment and operating and maintenance costs.

Emergoenvironmental analysis

Similar to exergoeconomic and emergoeconomic assessments, the emergoenvironmental analysis is grounded on the SPECO methodology [32]. The formulation used to perform the emergoenvironmental analysis is presented in Table 5.

In Table 5, $\dot{V}_k^{CO}$, $\dot{V}_k^{OM}$ and $\dot{V}_k^{DI}$ indicate the environmental emergy rate in the construction, operation and maintenance, and disposal phases, respectively.

Multi-objective optimization approach

For determining the optimal operating conditions of the proposed polygeneration system, GA-based multi-objective optimization is performed with the aid of the optimization toolbox in MATLAB software. The multi-objective approach is a valuable tool to evaluate the optimal solution of the main decision variables (DVs) when different objective functions (OFs) are considered simultaneously. In this study, the GA-based multi-objective approach consists of an integration of the ANN and GP to solve different OFs as function of main process DVs. ANN is a computing modelling method based on an assembly of artificial neurons, each one representing a specific output function known as activation function. Moreover, the memory of the ANN model is represented by the weight of each connection between two network neurons [36]. On the other hand, GP is an optimization technique founded on Darwin's evolution theory, which can be used to optimize the ANN model weights.

Fig. 2 depicts the flowchart of the developed optimization process. In this methodology, the initial random population is generated by applying crossover and mutation operators. In each iteration, the dominated solutions that do not meet the quality of OFs are discarded while non-dominated solutions that meet the criteria enter the next step of the pseudocode. Initial population size and mutation functions as the
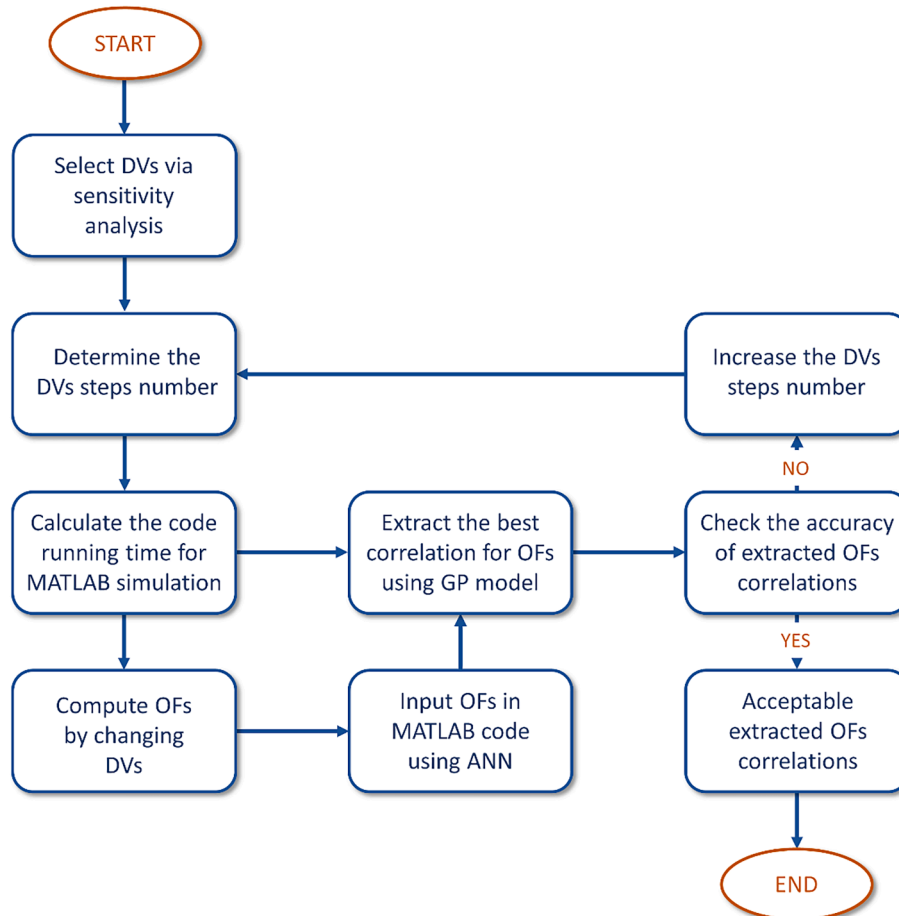

Fig. 2. Flowchart of the proposed multi-objective optimization procedure based on Artificial Neural Network (ANN) and Genetic Programming (GP).

Table 6

Objective functions for the three-objective optimization of the integrated solar energy-driven polygeneration and CO_2 capture system.

Objective Function	Symbol	Unit
Total cost rate	$\dot{C}_{TOT}$	US\$/h
Total environmental impact rate	$\dot{B}_{TOT}$	mPts/s
Total environmental emergy rate	$\dot{N}_{TOT}$	sej/h

Table 7

Objective functions for the four-objective optimization of the integrated solar energy-driven polygeneration and CO_2 capture system.

Objective Function	Symbol	Unit
Total cost rate	$\dot{C}_{TOT}$	US\$/h
Total environmental impact rate	$\dot{B}_{TOT}$	mPts/s
Total environmental emergy rate	$\dot{N}_{TOT}$	sej/h
The total economic emergy rate	$\dot{M}_{TOT}$	sej/h

Table 8

Objective functions for the six-objective optimization of the humidification-dehumidification (HDH) desalination unit.

Objective Function	Symbol	Unit
Exergy efficiency of the HDH unit	$\eta_{ex,TOT,HDH}$	%
Total cost rate	$\dot{C}_{TOT,HDH}$	US\$/h
Total environmental impact rate	$\dot{B}_{TOT,HDH}$	mPts/s
The total economic emergy rate	$\dot{M}_{TOT,HDH}$	sej/h
Total environmental emergy rate	$\dot{N}_{TOT,HDH}$	sej/h
Freshwater production rate	$Freshwater$	kg/s.m^2

Table 9

Decision variables of the proposed integrated solar energy-driven polygeneration and CO_2 capture system.

	Decision Variable	Symbol	Range	Unit
1	ORCHX1 pinch temperature difference	$T_{pinch,ORCHX1}$	100 – 200	°C
2	EVA pinch temperature difference	$T_{pinch,EVA}$	10 – 30	°C
3	Solar fraction	SF	0.25 – 0.95	–
4	Superheater outlet temp.	$T_{SUP,out}$	450 – 550	°C
5	Steam turbine isentropic efficiency	$\eta_{is,ST}$	70 – 90	%
6	Isentropic efficiency of ORCT1	$\eta_{is,ORCT1}$	70 – 90	%
7	ORCHX2 pinch temperature difference	$T_{pinch,ORCHX2}$	2 – 4	°C
8	Humidifier inlet hot water temperature	T_{Lh}	60 – 70	°C
9	Dehumidifier inlet cold water temperature	T_{Ld}	20 – 30	°C
10	Humidifier inlet hot water mass flowrate	L_h	0.7 – 0.9	kg/s.m^2
11	Dehumidifier inlet cold water mass flowrate	L_d	1 – 1.5	kg/s.m^2
12	Packing bed height	Z	0.5 – 1.5	m
13	Inlet dry air mass flowrate	G_h	0.25 – 0.75	°C

parameters of the GP should be determined before the optimization process. It should be noted that a reduced population size can easily identify the optimal solution, whereas oversized population can cause divergence from the optimum.

In this study, the optimization is conducted separately for the integrated solar-assisted polygeneration system and the HDH desalination unit. In this way, three and four objective functions are implemented for optimizing the proposed integrated polygeneration system as shown in Table 6 and Table 7, respectively. In addition, a six-objective functions

optimization is performed for the HDH desalination unit as shown in Table 8.

The main decision variables of the proposed polygeneration system model are presented in Table 9. Finally, the Pareto frontier optimal solutions are obtained for the objective functions made up with the optimal decision variables. In a six-dimensional space, the distance between the optimal point from any other point on the Pareto frontier is given by the following equation [37].

$$d_i = \sqrt{\begin{array}{l}\left(OF_1 - OF_{1,ideal}\right)^2 + \left(OF_2 - OF_{2,ideal}\right)^2 + \left(OF_3 - OF_{3,ideal}\right)^2 \\ + \left(OF_4 - OF_{4,ideal}\right)^2 + \left(OF_5 - OF_{5,ideal}\right)^2 + \left(OF_6 - OF_{6,ideal}\right)^2\end{array}}\Bigg|_i \tag{2}$$

Eq. (3) is used for the de-dimension of objective functions in the Pareto frontier optimal solutions [38]. This equation allows for eliminating the impact of dimensions of the different objective functions.

$$F_{ij} = \frac{f_{ij} - min_{i \in m}f_{ij}}{max_{i \in m}f_{ij} - min_{i \in m}f_{ij}} \tag{3}$$

Where f_{ij} indicates the ith value of the jth objective in the objective matrix, while F_{ij} corresponds to f_{ij} after normalization.

Results and discussion

Energy analysis

The mathematical modelling and simulation of the proposed integrated solar energy-driven polygeneration and CO_2 capture system is performed in MATLAB software. The results are validated via THERMOFLEX software. The obtained thermodynamic properties –including mass flowrates, temperatures, and pressures of each process stream– from the MATLAB model and THERMOFLEX simulation are compared in Table B.1 (see **Appendix B**). As shown in Table B.1, the validation results show high accuracy for June (summer season). In addition, Table B.2 (**Appendix B**) depicts the validation results related to the HDH desalination unit obtained from the developed MATLAB code compared with previous literature studies. As the validation results in Table B.2 reveal, the HDH desalination unit is also modelled and simulated accurately with negligible errors. In addition, Table B.3 presents the validation results obtained for main decision variables, including power production, power consumption and heat load of different system components. Once again, the results show high accuracy for the thermodynamic outputs obtained from the MATLAB model and THERMOFLEX simulation.

Sensitivity analysis

Sensitivity analysis is performed to better comprehend the influence of various parameters on the integrated system performance. Thus, sensitivity analysis allows evaluating the effect of the most critical variables on the thermodynamic, exergy, economic, and environmental performances of the system. In this regard, the most influential variables are selected to determine their magnitude and effect on the optimal performance solution, including the increase of power production and the reduction of costs and environmental impacts. The studied system parameters in this analysis are the pinch temperature of the ORC heat exchanger 1 (ORCHX1), pinch temperature of the evaporator (EVA), solar fraction, superheater (SUP) outlet temperature, and the isentropic efficiency of the steam turbine 1 (ST1). Hence, sensitivity analysis is conducted on some equipment units of the system, while the effect of the most important and influential system variables on the selected objective functions are illustrated in Fig. 3 to Fig. 14.

As shown in Fig. 3 to Fig. 5, the decision variables total cost rate $\dot{C}_{ToT}$, total environmental impact rate $\dot{B}_{ToT}$, total environmental emergy rate $\dot{N}_{ToT}$, and total economic emergy rate $\dot{M}_{ToT}$ increase with rising the pinch

Fig. 3. Sensitivity analysis of the decision variables $\dot{C}_{ToT}$ and $\dot{B}_{ToT}$ of the proposed integrated polygeneration system to the pinch temperature of the ORCHX1 unit.

Fig. 5. Sensitivity analysis of the decision variable $\dot{W}_{net}$ of the of the proposed integrated polygeneration system to the pinch temperature of the ORCHX1 unit.

temperature of the ORCHX1. In this way, Fig. 3 shows that $\dot{C}_{ToT}$ increases from 0.14 US\$/s to 0.235 US\$/s whilst $\dot{B}_{ToT}$ increases from 16.1 mPts/s to 16.9 mPts/s when the desired ORCHX1 pinch temperature changes from 60°C to 160°C. In this case, both $\dot{C}_{ToT}$ and $\dot{B}_{ToT}$ are improved due to the decreasing in the heat exchanger surface area as the pinch temperature of ORCHX1 diminishes, which in turn reduces the cost of purchasing equipment and increases energy costs.

From Fig. 4, it can be observed that both total environmental emergy rate $\dot{N}_{ToT}$, and total economic emergy rate $\dot{M}_{ToT}$ increase with the rising in the pinch temperature of the ORCHX1. Thus, by rising the pinch temperature of the ORCHX1 from 60°C to 160°C, $\dot{N}_{ToT}$ increase from 2.225 sej/s to 2.34 sej/s while $\dot{M}_{ToT}$ from 2.24 sej/s to 2.4 sej/s. These results are also due to the energy cost predominance as explained before. However, it is also observed in Fig. 5 that the net power production $\dot{W}_{net}$ decreases with the rise in the ORCHX1 pinch temperature. Moreover, the increase in the pinch temperature also causes the temperature and mass flowrate of the organic fluid to decrease, along with the production
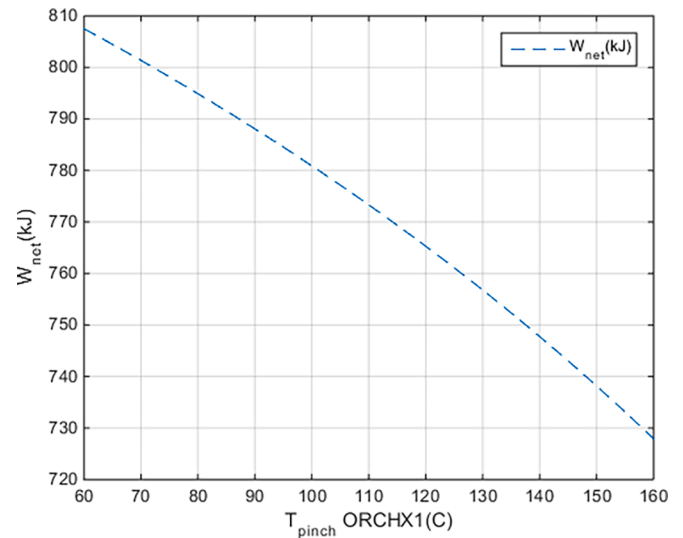
capacity of the ORC turbine. Therefore, the increase in the pinch temperature of the ORCHX1 will not favorably affect the system's thermodynamic, economic, and environmental performances.

Fig. 6 and Fig. 7 depict the results from the sensitivity analysis of the decision variables total cost rate $\dot{C}_{ToT}$, total environmental impact rate $\dot{B}_{ToT}$, total environmental emergy rate $\dot{N}_{ToT}$, and total economic emergy rate $\dot{M}_{ToT}$ to the pinch temperature of the evaporator (EVA) unit. According to these results, $\dot{C}_{ToT}$ and $\dot{M}_{ToT}$ increase because of the rise in the in pinch temperature of the EVA unit. However, the opposite behavior is observed for $\dot{B}_{ToT}$ and $\dot{N}_{ToT}$ which reduce with the EVA's pinch temperature increase. For instance, Fig. 6 shows that $\dot{C}_{ToT}$ increase from 0.199 US\$/s to 0.143 US\$/s while $\dot{B}_{ToT}$ decreases from 17.2 mPts/s to 16.4 mPts/s when EVA's pinch temperature changes from 2°C to 100°C. Fig. 7 indicates that $\dot{M}_{ToT}$ increases from 2 sej/s to 2.5 sej/s whilst $\dot{N}_{ToT}$ reduces from 2.336 sej/s to 2.253 sej/s with the rising in the EVA's pinch temperature.

It should be observed that the rise in this pinch temperature will

Fig. 4. Sensitivity analysis of the decision variables $\dot{N}_{ToT}$ and $\dot{M}_{ToT}$ of the proposed integrated polygeneration system to the pinch temperature of the ORCHX1 unit.
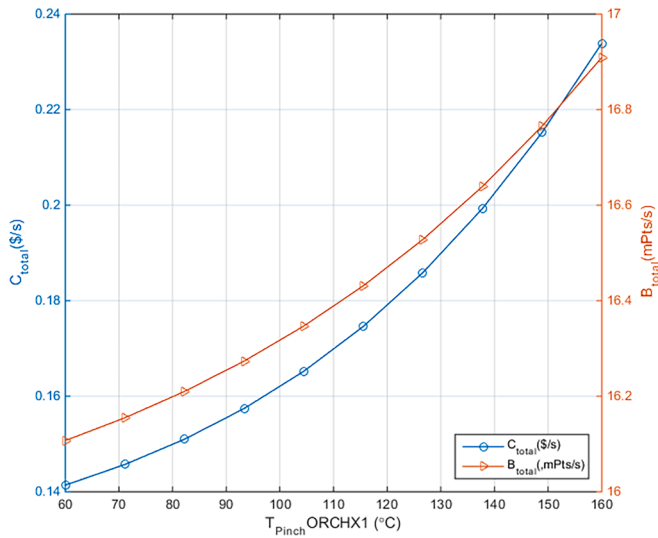

Fig. 6. Sensitivity analysis of the decision variables $\dot{C}_{ToT}$ and $\dot{B}_{ToT}$ of the proposed integrated polygeneration system to the pinch temperature of the evaporator (EVA) unit.
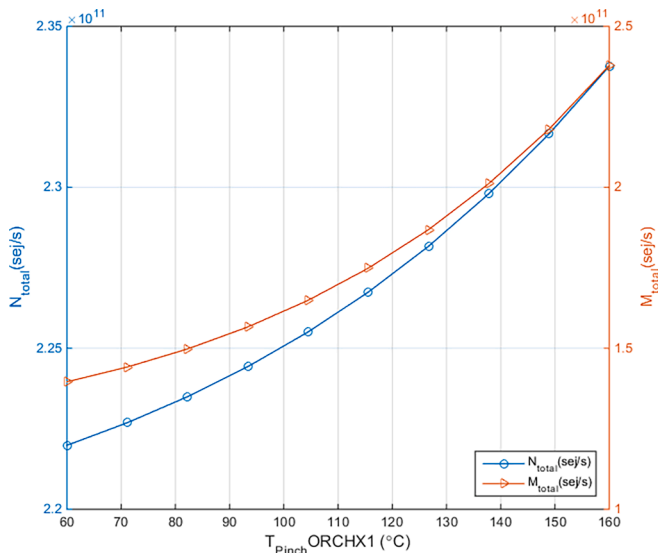
Fig. 7. Sensitivity analysis of the decision variables $\dot{N}_{ToT}$ and $\dot{M}_{ToT}$ of the proposed integrated polygeneration system to the pinch temperature of the evaporator (EVA) unit.

increase the temperature of flue gases exiting from the EVA. As a result, the total environmental impact rate $\dot{B}_{ToT}$ and total environmental emergy rate $\dot{N}_{ToT}$ tend to decrease. As observed in Table A.4, the weight of the EVA is a function of the flue gas temperature that leaves this component. Thus, increasing the pinch temperature of this heat exchanger will decrease the investment cost and the size of the unit. Yet, the amount of energy recovered and therefore total cost rate will increase. These results suggest that it is necessary to determine an optimal operating point for the evaporator pinch temperature that can improve the system performance from economic, environmental, and thermodynamic perspectives.

Fig. 8, Fig. 9, and Fig. 10 show the sensitivity analysis results for the system decision variables $\dot{C}_{ToT}$, $\dot{B}_{ToT}$, $\dot{N}_{ToT}$, $\dot{M}_{ToT}$, and $\dot{W}_{net}$ to the solar fraction. The results reveal that the rising in the solar fraction increases all five objective functions. It should be noted that increasing the solar fraction means that a higher flow rate of heat transfer fluid is required through the solar energy field. The latter ultimately leads to an increase in the mass flowrate of the ORC working fluid and, consequently, in the

system power generation. However, higher solar fractions will also adversely affect the integrated system's economic and environmental performances. Therefore, these results indicate the need to determine an optimal value for the solar fraction.

Fig. 11, Fig. 12, and Fig. 13 depict the sensitivity analysis results for the system decision variables $\dot{C}_{ToT}$, $\dot{B}_{ToT}$, $\dot{N}_{ToT}$, $\dot{M}_{ToT}$, and $\dot{W}_{net}$ to the SUP outlet temperature. As shown in these figures, the decision variables $\dot{C}_{ToT}$, $\dot{M}_{ToT}$, and $\dot{W}_{net}$ increase with the SUP outlet temperature rising while $\dot{B}_{ToT}$ and $\dot{N}_{ToT}$ decrease. These results suggest that determining an optimal operating point for the SUP outlet temperature can enhance the system performance from economic, environmental, and thermodynamic standpoints. Finally, Fig. 14 shows that $\dot{W}_{net}$. increases linearly with the ST1 isentropic efficiency rising. The irreversibility and, thereby, the exergy destruction of the turbine reduces with the increase in the isentropic efficiency. The latter will lead to increased power production.

Fig. 9. Sensitivity analysis of the decision variables $\dot{N}_{ToT}$ and $\dot{M}_{ToT}$ of the proposed integrated polygeneration system to the solar fraction.

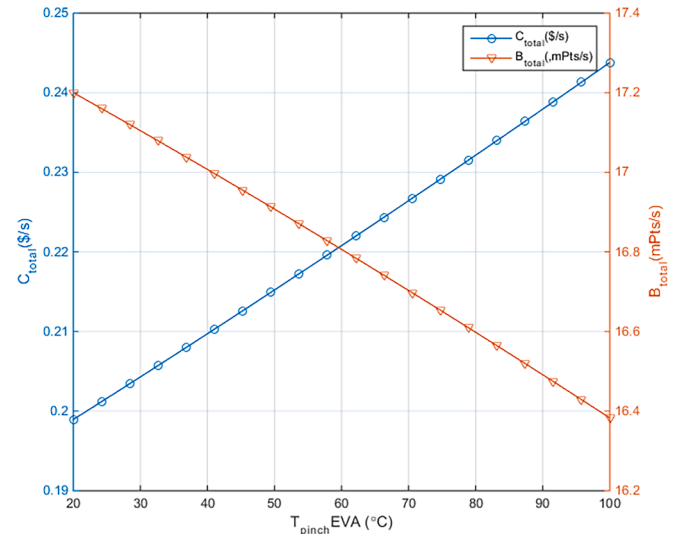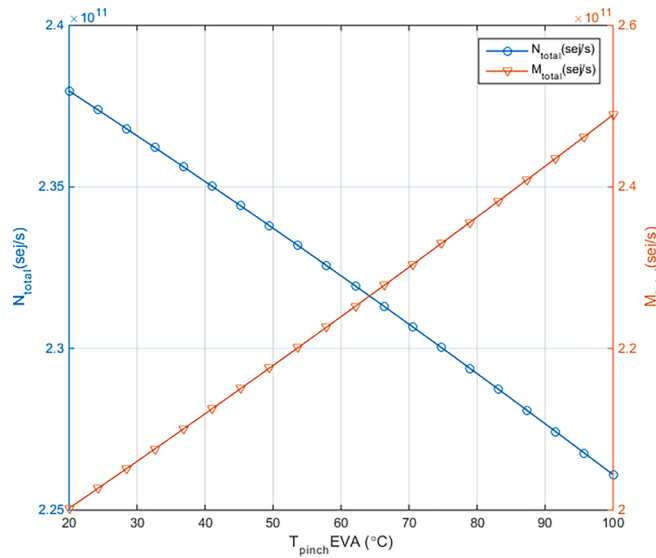**Fig. 8.** Sensitivity analysis of the decision variables $\dot{C}_{ToT}$ and $\dot{B}_{ToT}$ of the proposed integrated polygeneration system to the solar fraction.
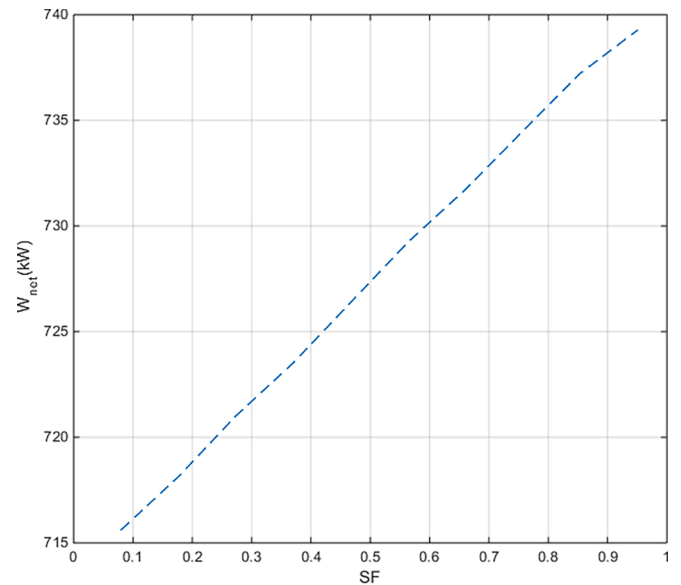
Fig. 10. Sensitivity analysis of the decision variable $\dot{W}_{net}$ of the proposed integrated polygeneration system to the solar fraction.

Fig. 11. Sensitivity analysis of the decision variables $\dot{C}_{ToT}$ and $\dot{B}_{ToT}$ of the proposed integrated polygeneration system to the superheater (SUP) outlet temperature.
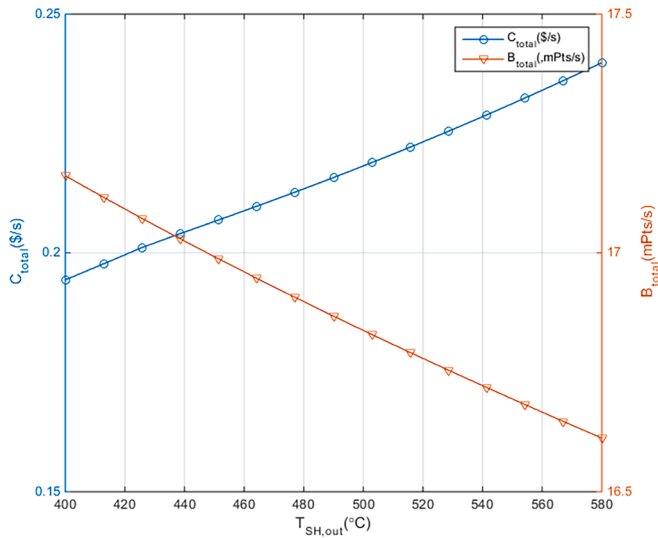
Fig. 13. Sensitivity analysis of the decision variable $\dot{W}_{net}$ of the proposed integrated polygeneration system to the superheater (SUP) outlet temperature.
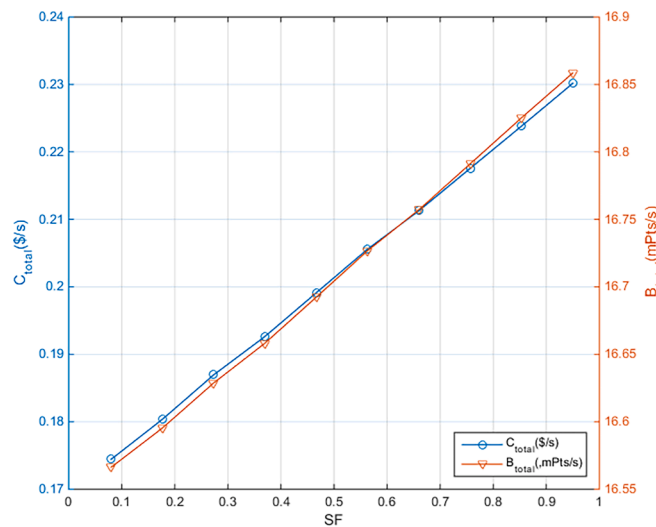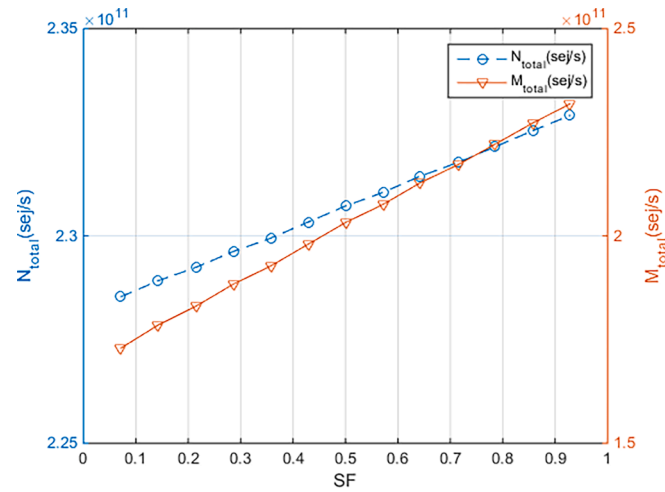

Fig. 12. Sensitivity analysis of the decision variables $\dot{N}_{ToT}$ and $\dot{M}_{ToT}$ of the proposed integrated polygeneration system to the superheater (SUP) outlet temperature.
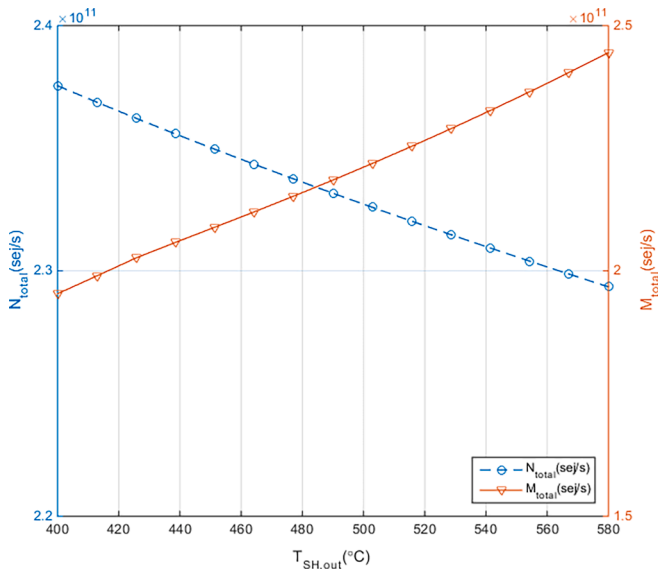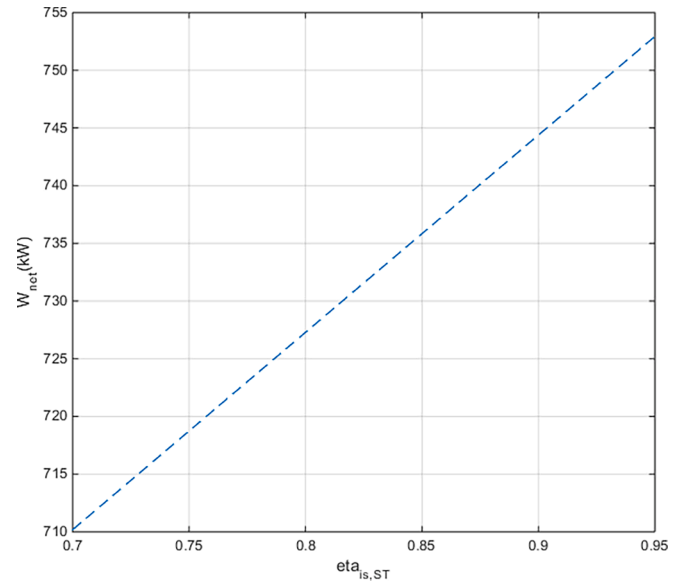
Fig. 14. Sensitivity analysis of the decision variable $\dot{W}_{net}$ of the proposed integrated polygeneration system to the steam turbine 1 (ST1) isentropic efficiency.

Optimization results

This section presents the results from the three and four-objective optimization of the integrated solar-assisted polygeneration and CO_2 capture system and the six-objective optimization performed for the HDH desalination unit. The objective functions correlations extracted by the GA-based model for the proposed polygeneration system integrated with solar energy field and CO_2 capture unit are listed in Table 10 for June (summer). Table 11 shows the corresponding extracted correlations for six-objective optimization of the HDH desalination unit.

The results of multi-objective optimization of the integrated system are determined based on the distance concept [37]. In this way, the closest solution to the optimal point solutions in the Pareto frontier is considered for both objective functions and decision variables. The optimal solutions for objective functions and decision variables of the integrated polygeneration system when three objective functions are

under consideration are shown in Table 12 and Table 13, respectively. As shown in Table 12, the implementation of three-objective optimization method reduces the total system costs, environmental impacts, and total monthly environmental emergy rate by 11.4%, 34.31% and 6.38%, respectively. The results from Table 13 indicate that all the decision variables are reduced via optimization, which enhances the objective functions, including the total system costs, environmental impacts, and total monthly environmental emergy. In this case, the overall cycle efficiency is increased from 34% to 34.9% after optimization.

Fig. 15 displays the corresponding Pareto frontier diagrams of the three-objective optimization. A set of optimal solutions are formed by discarding the dominated solutions, as shown in Fig. 15. Then, a solution superior to the rest of the search space is chosen as the optimal solution. It should also be noted that an optimal solution minimizes all the objective functions at once. The point where both objective functions are

Table 10
Extracted correlations by the genetic algorithm (GA) approach for the proposed integrated solar energy-driven polygeneration and CO_2 capture system.

Objective Function (Units)	Correlation	R^2
$\dot{C}_{TOT}$ $\left(\dfrac{US\$}{kW}\right)$	$0.1055780499980218 + 1.9820651588994 \times 10^{-9}\Delta T^4_{pinch,EVA} \times 105.3469071626697^{cosSF} \times \left(1.016041949975967 + \dfrac{-2.53820729068}{\Delta T_{pinch,ORCHX1}}\right)^{1031.1559207829I} cos\Delta T_{pinch,EVA}$	0.86
$\dot{B}_{TOT}$ $\left(\dfrac{mpts}{kW}\right)$	$12.6224172159888SF + 11.388706846366 \dfrac{cos(cos\Delta T_{pinch,EVA} + cos\Delta T_{pinch,ORCHX1}\sqrt{log\Delta T_{pinch,EVA}})}{SF} + 6.26617319981566cos(log\Delta T_{pinch,EVA} + cos(2.123512488592 + log\Delta T_{pinch,EVA} \times cos(cos\Delta T_{pinch,EVA} \times \sqrt{log\Delta T_{pinch,EVA}})))$	0.96
$\dot{M}_{TOT}$ (sej/s)	$206148967191.794/(2.00842013424532cos\Delta T_{pinch,ORCHX1}sin\Delta T_{pinch,EVA} \times SF) + 28643128282 0.84/(1.97870330779311cos\Delta T_{pinch,ORCHX1}^2\Delta T_{pinch,ORCHX1}0.94068951373 + SF + \Delta T_{pinch,EVA}SF^2) - 449120591244.199$	0.98
$\dot{N}_{TOT}$ (sej/s)	$13323671580.1318\Delta T_{pinch,ORCHX1} + (5380371605.2027/sin\Delta T_{pinch,ORCHX1}^2) + 10924171864 01.91sin\Delta T_{pinch,ORCHX1}^2sin(\Delta T_{pinch,ORCHX1})/SF) + 2801459627316.42sin\Delta T_{pinch,EVA}^2 \Delta T_{pinch,EVA} + 13323671580.1318\Delta T_{pinch,ORCHX1} + 13323671580.1318\Delta T_{pinch,ORCHX1} + 5380371605.2027/sin\Delta T_{pinch,ORCHX1}^2\Delta T_{pinch,ORCHX1} + (-305343924052 3.61sin\Delta T_{pinch,ORCHX1}^2) + 13323671580.1318\Delta T_{pinch,ORCHX1} + 5380371605.2027/sin\Delta T_{pinch,ORCHX1}^2) - 1267215622594.89$	0.86

in the best state is called the ideal point. Hence, to select the optimal point, one should choose a point from the set of Pareto points with the smallest distance to the ideal point. In this way, Fig. 15(a) and 15(c) reveal that by increasing the total environmental emergy rate, the total monthly environmental impact rate does not change considerably while the total system cost increases. On the other hand, Fig. 15(b) shows that the total system cost increases with the rising in the total monthly environmental impact rate.

Table 14 and Table 15 present the optimal solutions obtained for objective functions and decision variables when four objective functions are considered for optimizing the integrated solar-assisted polygeneration and CO_2 capture system. The results in Table 14 indicate that the four-objective optimization of the proposed system reduces the total costs, environmental impacts and the total monthly environmental emergy rate by 56.81%, 50.19% and 77.07%, respectively. However, the total monthly economic emergy rate is increased when compared to the base case. The aid of revised decision variables can achieve an optimal result. From the results of Table 15, it can be concluded that an increase in $\Delta T_{pinch,ORCHX2}$ and decreases in remaining decision variables can help to boost the performance of the cycle. In this case, the cycle's overall system efficiency and exergy efficiency are changed to 34.08% and 31.7%, respectively.

Fig. 16 displays the Pareto frontier diagrams obtained for the four objective functions and the relationship between objective functions of the proposed system. As explained before, the optimal solution is selected by considering the type of objective function (to be minimized or maximized via optimization). In this case, all the selected objective functions should be minimized. For example, as shown in Fig. 16(a), the optimal solution that minimizes the objective functions, i.e., the one that has the smallest distance to the origin of the coordinate system, presents $\dot{C}_{TOT}$ equal to 0.8 US$/s and $\dot{B}_{TOT}$ at 12 mPts/s, respectively.

Table 16 and Table 17 show the optimal solutions obtained for objective functions and decision variables when six objective functions are considered for optimizing the HDH desalination unit. As indicated in Table 16, the multi-objective optimization of the HDH unit results in the enhancement of its exergy efficiency by 7.3%. Moreover, the total system costs, environmental impacts, total monthly economic emergy rate, and the total monthly environmental emergy rate of the HDH unit are reduced by 36%, 40%, 36.6% and 40%, respectively. The results from Table 17 indicate that an increase in $T_{Gh,in}$ and $L_{d,in}$ and a decrease in remaining decision variables should be considered for achieving the optimal system's operation.

Fig. 17 depicts the Pareto frontier diagrams obtained for the six objective functions and the relationship between objective functions of the HDH unit.

Fig. 17(a) depicts the Pareto optimal solution frontier for the decision variables $\dot{M}_{TOT}$, $\dot{C}_{TOT}$, and HDH exergy efficiency $\eta_{ex,TOT,HDH}$. As demonstrated in this diagram, the decision variables $\dot{C}_{TOT}$ and $\dot{M}_{TOT}$ are increased with the decreasing of the HDH exergy efficiency from 62 to 52%. Moreover, Fig. 17(b) shows that the decision variable $\dot{N}_{TOT}$ is increased when $\eta_{ex,TOT,HDH}$ is decreased. Fig. 17(c) displays the Pareto optimal solution frontier for the decision variables $\dot{M}_{TOT}$, $\dot{N}_{TOT}$, and $\eta_{ex,TOT,HDH}$. This diagram shows that $\dot{M}_{TOT}$ and $\dot{N}_{TOT}$ increase with decreasing the exergy efficiency of HDH unit. Fig. 17(d) illustrates the optimal Pareto solution frontier for the decision variables $\dot{B}_{TOT}$, $\eta_{ex,TOT,HDH}$, and freshwater production. In this case, freshwater production and $\dot{B}_{TOT}$ are increased with decreasing the exergy efficiency of the HDH unit. Fig. 17(e) demonstrates that with decreasing the HDH exergy efficiency, the freshwater production and $\dot{C}_{TOT}$ are increased. Moreover, with decreasing the HDH exergy efficiency, $\dot{M}_{TOT}$ is reduced as shown in Fig. 17(f), and $\dot{B}_{TOT}$ is decreased as indicated in Fig. 17(g).

Fig. 17(h) shows the Pareto optimal solutions for the decision variables $\dot{M}_{TOT}$, $\dot{C}_{TOT}$, and freshwater production. As shown, $\dot{M}_{TOT}$ and $\dot{C}_{TOT}$ increase with rising the freshwater production. In addition, $\dot{N}_{TOT}$ is also

Table 11
Extracted correlations by the genetic algorithm (GA) approach for the humidification-dehumidification (HDH) desalination unit.

Objective Function (Units)	Correlation	R^2
$eta_{ex,TOT,HDH}$	$1.3852827052572 + 0.186772873327336 L_{d,in} Z + 0.345880148263565 G L_{d,in}^2 - 0.00737645036312701 T_{Lh,in} - 0.0594873354164552 Z - 0.384550916237678 L_{d,in} G - 0.0527931913239205 L_{d,in} G - 0.6725507653188662 G$	0.97
$\dot{C}_{TOT,HDH}\left(\dfrac{US\$}{kW}\right)$	$1.968741721487 \times 10^{-5} L_{h,in} L_{d,in} + 3.0393215478498 \times 10^{-10} T_{Lh,in}^3 + 5.0396653134050 4 \times 10^{-6} T_{Gh,in} GZ - 4.28962102194987 \times 10^{-5} ZG - 5.94302080241707 \times 10^{-5} - 3.2527418306788 \times 10^{-8} T_{Gh,in}$	0.97
$\dot{B}_{TOT,HDH}\left(\dfrac{mpts}{kW}\right)$	$0.00625024987039988 L_{h,in} + 6.42565050479867 \times 10^{-8} T_{Lh,in} + 0.0007300273961103339 T_{Gh,in} ZG - 0.0147719046351729 - 1.12869476924364 \times 10^{-7} T_{Gh,in}^3 - 0.0001261693376577661 L_{h,in} ZG$	0.96
$\dot{M}_{TOT,HDH}$ (sej/s)	$5815134.92009196 L_{d,in} Z + 26523.3179328334 T_{Lh,in}^2 + 2973121.97336974 T_{Gh,in} ZG - 7490872.1925363 - 5147785.55711537 9 T_{Gh,in}$	0.97
$\dot{N}_{TOT,HDH}$ (sej/s)	$39720280.7506605 Z + 11181648.0210332 T_{Lh,in} + 218110.345454342 ZT_{Lh,in}^2 - 623304221.495155 - 818786.0904700093 T_{Gh,in}$	0.98
Freshwater (kg/s.m²)	$0.031008532625834 L_{d,in} G + 0.0002369980711556187 T_{Gh,in} L_{d,in} Z + 4.64876223480212 \times 10^{-6} L_{h,in} T_{Lh,in}^2 - 0.00264710168661556 - 0.00284488366337111 L_{d,in} - 0.0436278489767814 ZG^2$	0.94

Table 12
Optimal design solution obtained for the three-objective optimization in June.

	$\dot{C}_{TOT}$ (US\$/s)	$\dot{B}_{TOT}$ (mpts/s)	$\dot{N}_{TOT}$ (sej/s)
Optimization	0.11	11.04	2.17×10^{11}
Base Case	0.2207	16.8082	2.32×10^{11}

improved with increasing the freshwater production as indicated in Fig. 17(i). In addition, the freshwater production rising also causes $\dot{N}_{TOT}$ and $\dot{B}_{TOT}$ to increase as shown in Fig. 17(j), as well as $\dot{N}_{TOT}$ and $\dot{C}_{TOT}$ in Fig. 17(k). On the other hand, Fig. 17(l) reveals that $\dot{C}_{TOT}$ and $\dot{B}_{TOT}$ are increased by reducing the exergy efficiency of the HDH unit. Fig. 17(m) demonstrates that $\dot{B}_{TOT}$, and $\dot{C}_{TOT}$ are increased by rising the freshwater production. The decision variables $\dot{B}_{TOT}$ and $\dot{N}_{TOT}$ are increased with increasing $\dot{C}_{TOT}$ as indicated in Fig. 17(n), while $\dot{M}_{TOT}$ is increased with the rising in the HDH exergy efficiency as shown in Fig. 17(o). Fig. 17(p) indicates that $\dot{M}_{TOT}$ is increased and $\dot{B}_{TOT}$ reduced with the increasing in the exergy efficiency of HDH unit. Finally, $\dot{M}_{TOT}$ and $\dot{B}_{TOT}$ are increased with the increasing in the freshwater production as indicated in Fig. 17 (q).

The energy efficiency of the proposed integrated polygeneration system after optimization is equal to 36.11% (which can reach 37.66% when polygeneration efficiency is considered). The reported amount for overall energy efficiency is improved when compared with Refs. [4,33,39–42] as follows. Dabwan et al. [4] reported an energy efficiency of approximately 27% (June) for a solar preheating gas turbine using parabolic trough collectors. The ORC system driven by parabolic trough collectors investigated by Yu et al. [39] improved the overall system efficiency from 17.9% to 24.8% utilizing the particle swarm optimization (PSO) algorithm. Furthermore, an electrical efficiency of 30.5% was reported by Gholizade et al. [40] for a trigeneration system composed of a GT cycle, cooling/electricity cogeneration system based on ORC and ejector cooling cycle (ECC), and HDH unit. The integration of PTC to the steam turbine of a combined cycle was investigated by Rovira et al. [41], with a thermal efficiency of 32.4%. Finally, Zhang et al. [42] developed a trigeneration system including power, heating, and freshwater based on parabolic trough solar collectors and the energy efficiency is reported as 34.78%.

The results of the 6E analyses of the proposed integrated solar energy-driven polygeneration and CO_2 capture system based on the four-objective optimization are presented in the following sections.

Exergy analysis

For a better understanding of each system component contribution for the total exergy destruction rate of the proposed cycle, a pie diagram is presented in Fig. 18. According to these results, the combustion chamber (CC) has the highest amount of exergy destruction compared to the other components, with 56% share due to the chemical reaction, followed by the CO_2 capture and HRSG units with 10% and 8% contribution, respectively. Moreover, the HDH desalination unit does not present contributions to the total exergy destruction rate of the system. Hence, it can be concluded that the HDH unit operates efficiently while its associated costs are insignificant.

Additionally, exergy features of each stream concerning to the proposed configuration based on the four-objective optimization are shown in the Sankey diagram in Fig. 19. As shown in Fig. 19, the equipment units related to the GT cycle consume the highest fuel exergy flow and the most exergy destruction compared to the remaining integrated power cycles. After that, a heat exchanger network for flue gas recovery can be considered the next priority for reducing fuel exergy consumption.

Table 13

Optimal solution obtained for the decision variables of the three objective functions optimization.

	$\Delta T_{pinch,ORCHX1}$ (°C)	$\Delta T_{pinch,EVA}$ (°C)	SF (−)	$T_{SUP,out}$ (°C)	$\eta_{is,ST}$ (−)	$\eta_{is,ORCT1}$ (−)	$\Delta T_{pinch,ORCHX2}$ (°C)
Optimization	134.12	50.38	0.34	544.5	0.87	0.8	3.06
Base Case	152.4	59.8	0.8	510	0.88	0.85	2.6

(a)

(b)

(c)
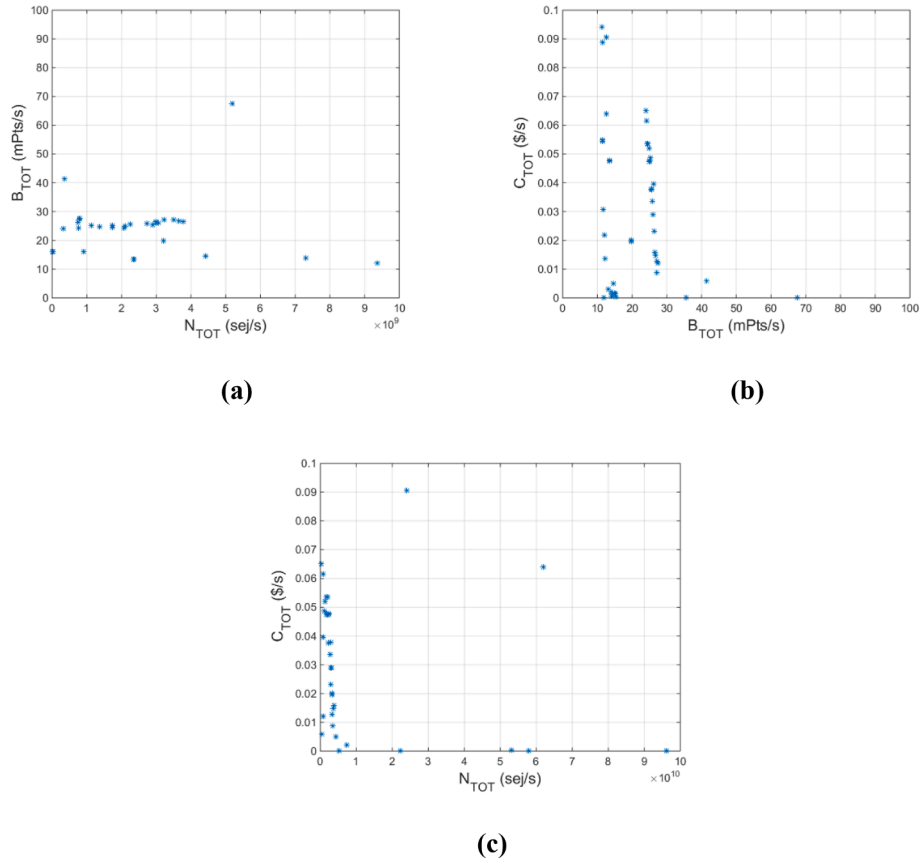
Fig. 15. Pareto frontier diagrams of the three-objective optimization of the proposed integrated polygeneration system showing the decision variables (*a*) $\dot{B}_{TOT}$ versus $\dot{N}_{TOT}$; (*b*) $\dot{C}_{TOT}$ versus $\dot{B}_{TOT}$; and, (*c*) $\dot{C}_{TOT}$ versus $\dot{N}_{TOT}$.

Table 14

Optimal design solution obtained for the four-objective optimization in June.

	$\dot{C}_{TOT}$ (US$/s)	$\dot{B}_{TOT}$ (mpts/s)	$\dot{M}_{TOT}$ (sej/s)	$\dot{N}_{TOT}$ (sej/s)
Optimization	0.095329	8.372616	4.29×10^{13}	5.32×10^{10}
Base Case	0.2207	16.8082	2.24×10^{11}	2.32×10^{11}

Table 15

Optimal solution obtained for the decision variables of the four objective functions optimization.

	$\Delta T_{pinch,ORCHX1}$ (°C)	$\Delta T_{pinch,EVA}$ (°C)	SF (−)	$T_{SUP,out}$ (°C)	$\eta_{is,ST}$ (−)	$\eta_{is,ORCT1}$ (−)	$\Delta T_{pinch,ORCHX2}$ (°C)
Optimization	136.38	59.82	0.44	505.9	0.86	0.75	3.31
Base Case	152.4	59.8	0.8	510	0.88	0.85	2.6

(a)

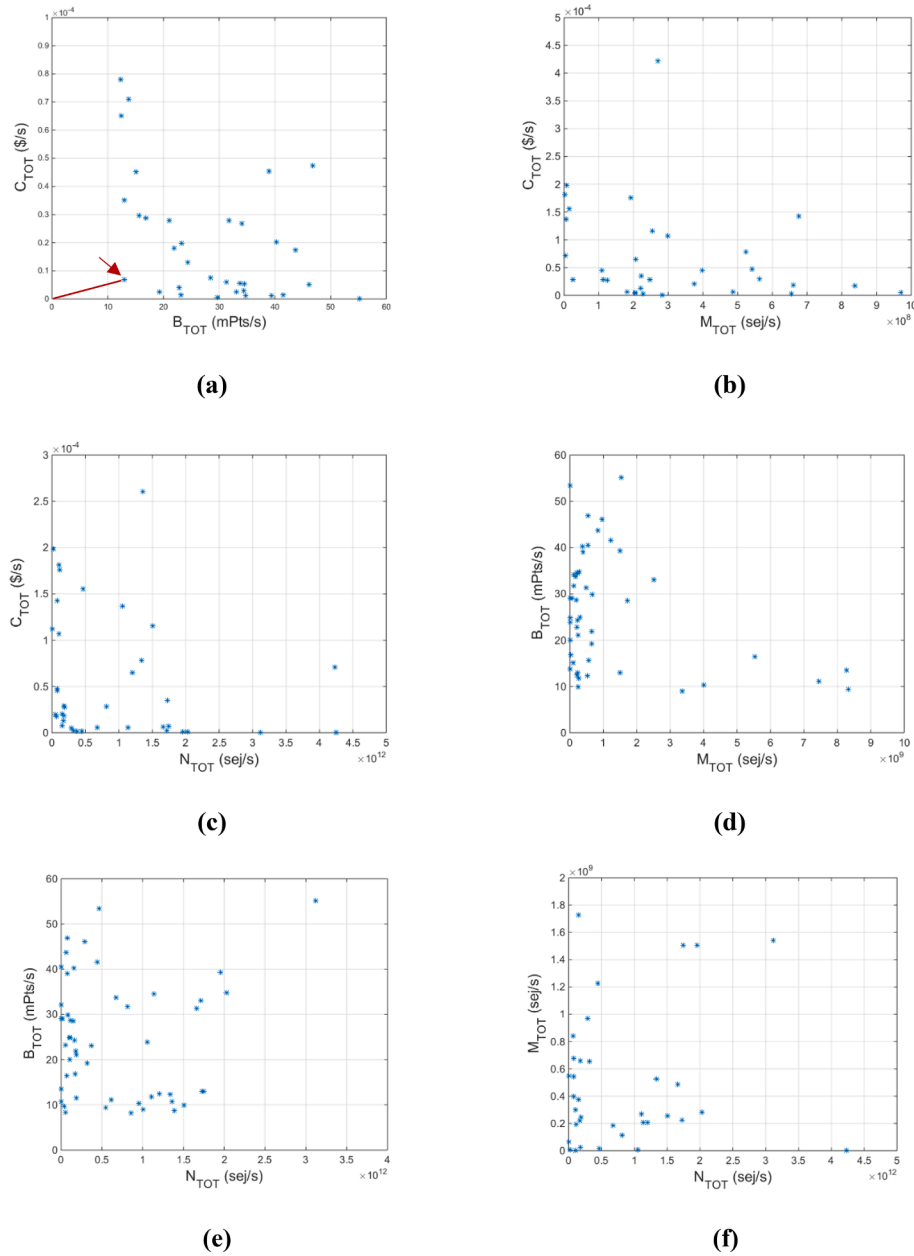
(b)

(c)

(d)

(e)

(f)

Fig. 16. Pareto frontier diagrams of the four objective functions of the proposed integrated polygeneration system.

Table 16
Optimal design solution obtained for the six-objective optimization of the HDH desalination unit in June.

	$\dot{C}_{TOT,HDH}$ (US$/s)	$\dot{B}_{TOT,HDH}$ (mpts/s)	$\dot{M}_{TOT,HDH}$ (sej/s)	$\dot{N}_{TOT,HDH}$ (sej/s)	$\eta_{ex,TOT,HDH}$ (−)	Freshwater (kg/s.m²)
Optimization	3.6×10^{-5}	0.006	3.33×10^{7}	8.57×10^{7}	0.59	0.201
Base Case	5.65×10^{-5}	0.01	5.25×10^{7}	1.43×10^{8}	0.55	0.0221

Table 17
Optimal solution obtained for the decision variables of the six-objective optimization for HDH desalination unit in June.

	$T_{Lh,in}$ (°C)	$T_{Gh,in}$ (°C)	$L_{h,in}$ (kg/s.m²)	$L_{d,in}$ (kg/s.m²)	Z (m)	G_h (kg/s.m²)
Optimization	62.1	28.3	0.84	1.05	0.61	0.28
Base Case	65.5	25	0.89	1	0.7	0.32
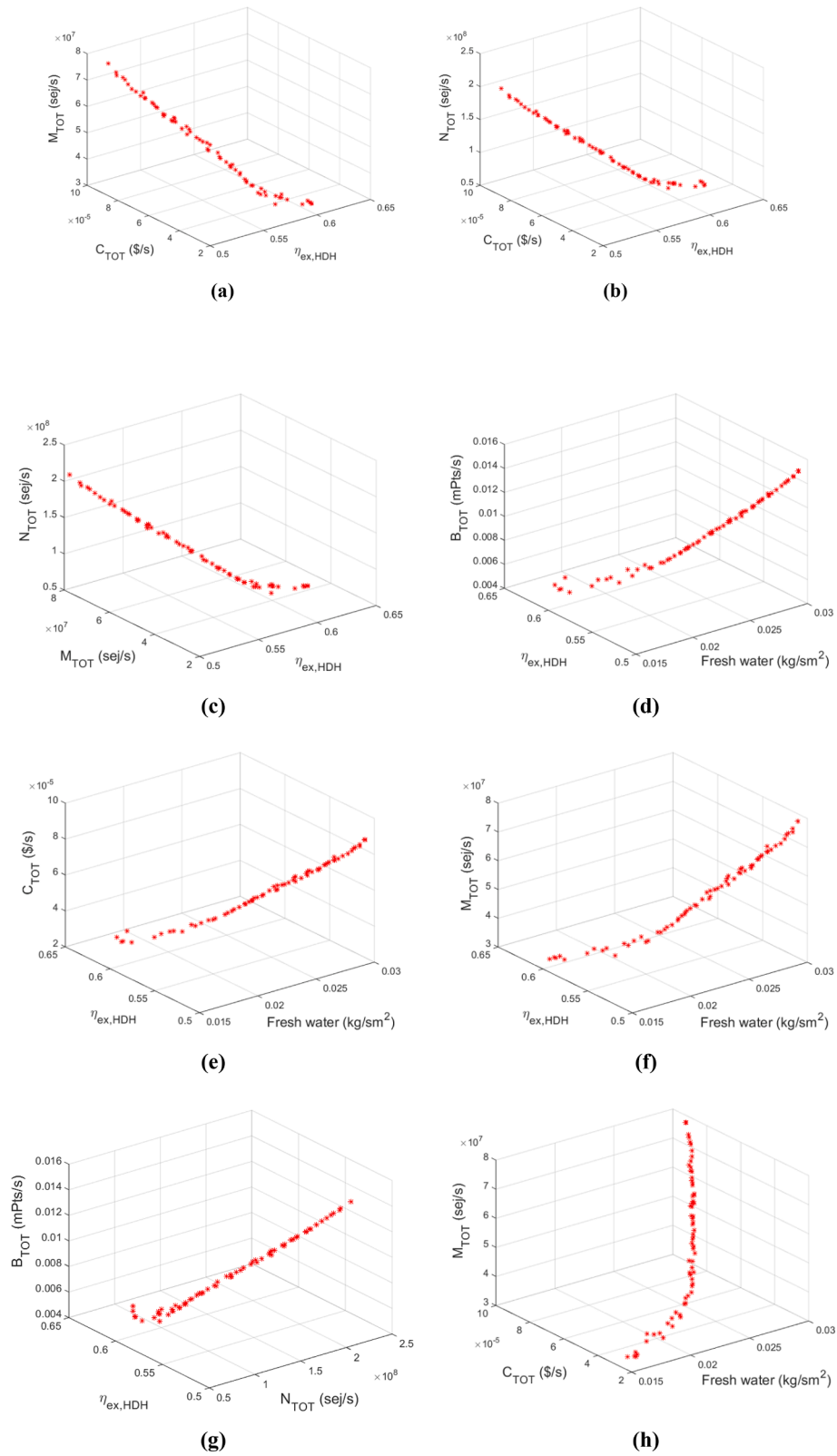
Fig. 17. Pareto frontier diagrams of the six objective functions of the HDH desalination unit.

(i)

(j)

(k)

(l)

(m)

(n)

(o)

(p)

(q)
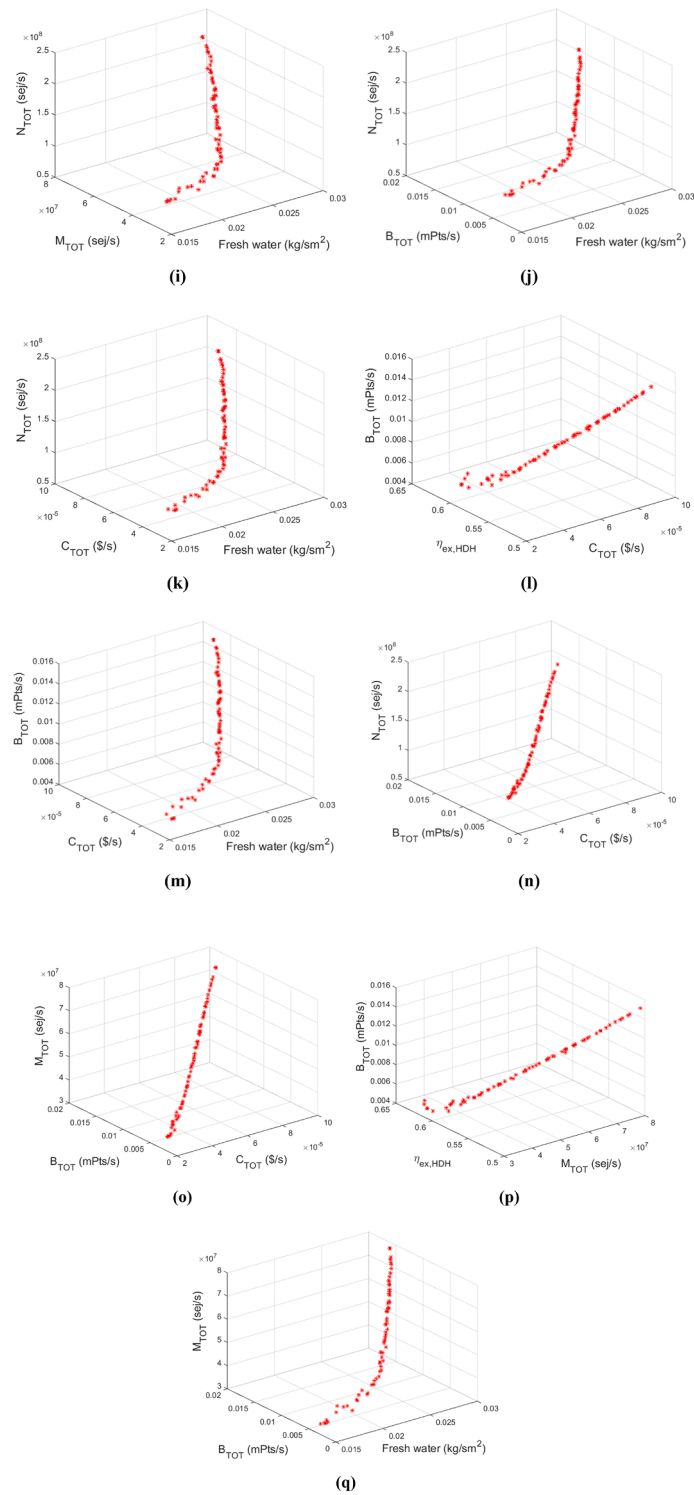
Fig. 17. (*continued*).
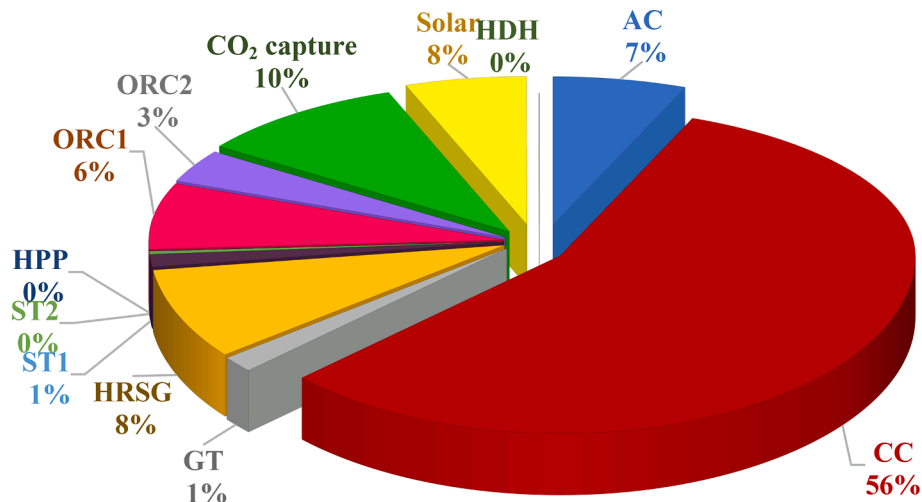
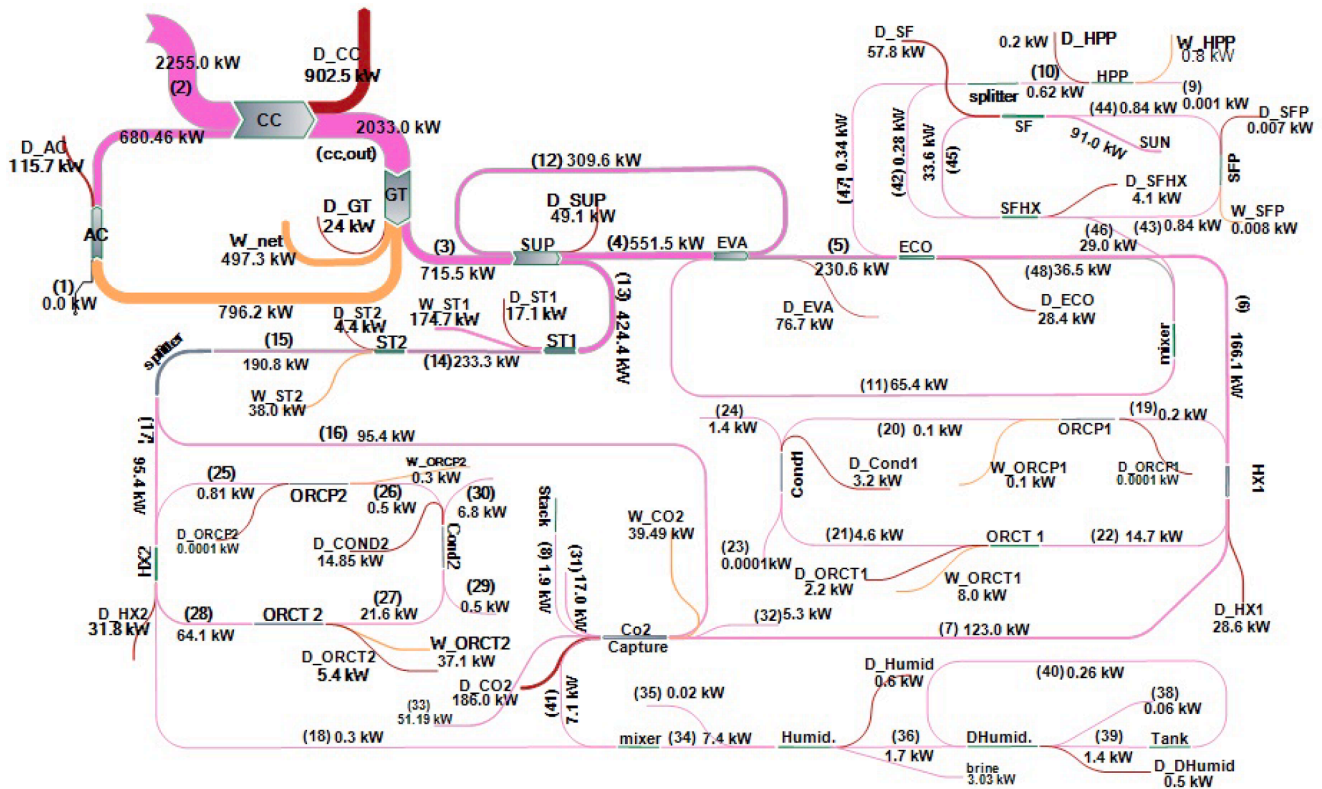**Fig. 18.** Exergy degradation contribution of each system component.

Fig. 19. Sankey diagram of the integrated polygeneration system related to the exergy analysis after the four-objective optimization.

Exergoeconomic analysis

As aforementioned, the exergoeconomic assessment is conducted for each element of the proposed integrated polygeneration system. This evaluation aims to determine the system components with the highest values for operating costs, exergy destruction rates and r_k factor and specify those elements that account for the lowest exergoeconomic factor. This analysis will allow to boost their performance and decrease

their exergy degradation on the function of the entire system by allocating more expenses (cost rate).

Fig. 20 illustrates the exergoeconomic Sankey diagram of the integrated system based on the four-objective optimization. The results reveal that the highest costs given by $\dot{Z}_k + \dot{C}_D$ are related to the CO_2 capture unit with 125.2 US\$/h, followed by the ORC heat exchanger 1 (43.9 US\$/h), and combustion chamber (41.3 US\$/h), respectively.
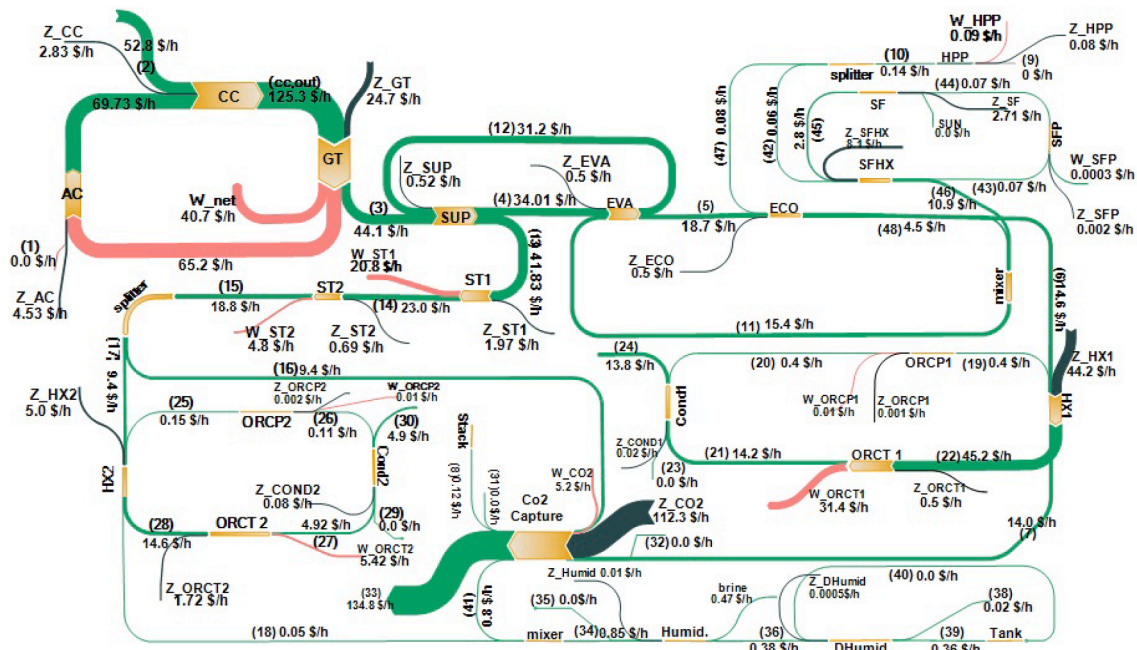
Fig. 20. Sankey diagram of the integrated polygeneration system related to the exergoeconomic analysis after the four-objective optimization.
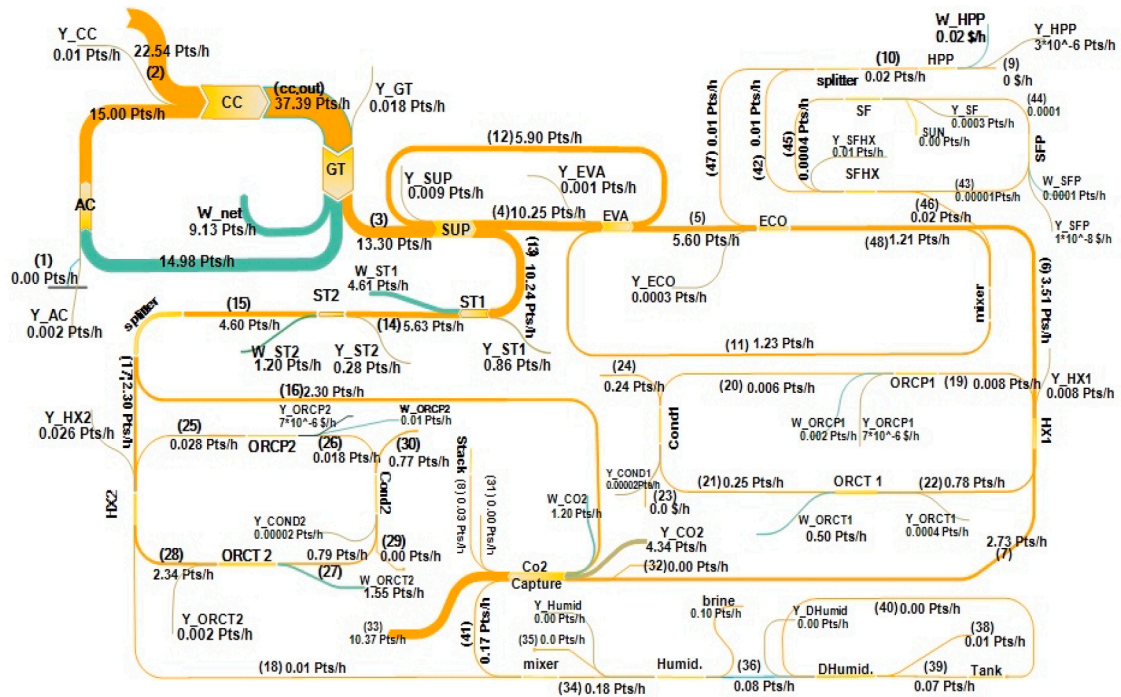

Fig. 21. Sankey diagram of the integrated polygeneration system related to the exergoenvironmental analysis after the four-objective optimization.

Exergoenvironmental analysis

The exergoenvironmental analysis allows for determining the environmental impacts of different subsystems during the manufacturing, transportation, and operation phases. Fig. 21 exhibits the exergoenvironmental Sankey diagram of the proposed integrated polygeneration system after the four-objective optimization. Referring to the obtained results, the highest environmental impact rate –as the summation of the environmental impacts related to each system unit $\dot{Y}_k$ and the exergy destruction $\dot{B}_D$– is allocated to the combustion chamber with 11,805

mPts/h, followed by the CO_2 capture unit (8843 mPts/h), and steam turbine 2 (1265.3 mPts/h), respectively.

Emergy evaluation

Emergoeconomic analysis

Fig. 22 depicts the emergoeconomic Sankey diagram of the integrated polygeneration system related to the emergoeconomic analysis after the four-objective optimization. The emergoeconomic evaluation results show that the highest total economic emergy rate $\dot{M}_D + \dot{U}_k$ is
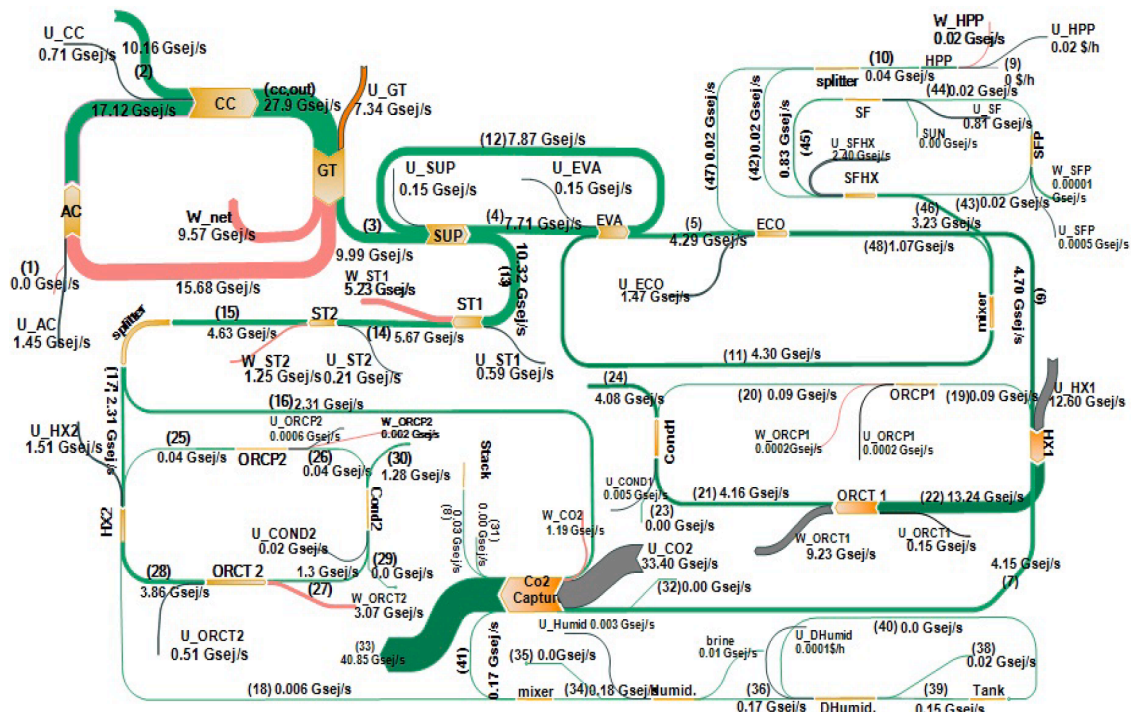
Fig. 22. Sankey diagram of the integrated polygeneration system related to the emergoeconomic analysis after the four-objective optimization.
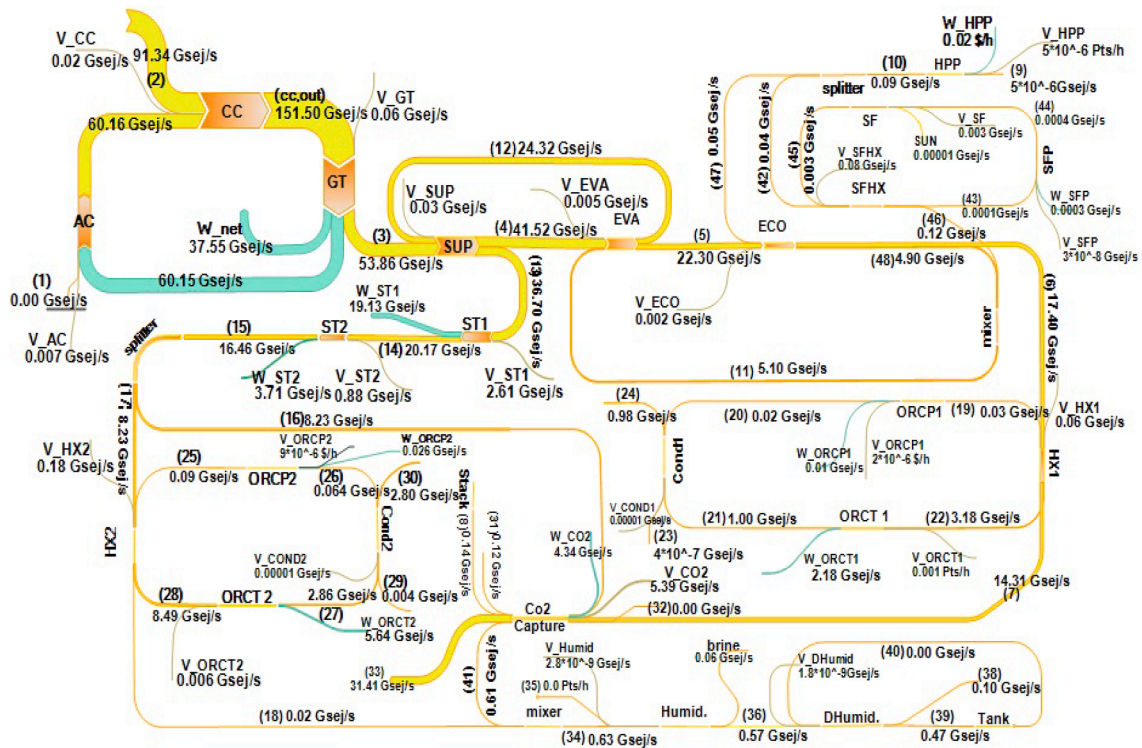

Fig. 23. Sankey diagram of the integrated polygeneration system related to the emergoenvironmental analysis after four-objective optimization.

related to the CO_2 capture unit with 1.34×10^{14} sej/h, followed by the combustion chamber (6.06×10^{13} sej/h) and the ORC heat exchanger 1 (4.65×10^{13} sej/h), respectively.

Emergoenvironmental analysis

Fig. 23 displays the emergoenvironmental Sankey diagram of the

integrated polygeneration system after the four-objective optimization. The results from the emergoenvironmental assessment reveal that the highest amount of total environmental emergy rate $\dot{N}_D + \dot{V}_k$ belongs to the combustion chamber with 1.68×10^{14} sej/h, followed by the CO_2 capture unit (8.15×10^{13} sej/h) and the ORC heat exchanger 1 (7.44×10^{12} sej/h), respectively.

Table A1
Modelling parameters of the solar ET-100 parabolic-trough collectors [43].

Modelling Parameter	Value
Absorber Radius	35 mm
Aperture Area	552 m^2
Aperture Width	5.76 m
Collector Length	99.5 m
Collector Modules Length	12 m
Focal Length	1.71 m
Mirror Reflectivity	94 %
Number of Modules per Drive	8
Number of Glass Facets	224
Number of Absorber Tubes	24
Parabolic Mirror Panels per Modules (horizontal $\times$ vertical)	28 (7 $\times$ 4)
Weight of Steel Structure and Pylons, per m^2 aperture	19 kg

Conclusions

This study introduces a new machine learning-based approach for the multi-objective optimization of an integrated solar energy-driven polygeneration and CO$_2$ capture system. The solar-assisted polygeneration system comprises gas and steam turbine cycles, organic Rankine cycles, humidification-dehumidification desalination, post-combustion CO$_2$ capture, and parabolic-trough solar collectors. The proposed integrated system is mathematically modelled and evaluated via a dynamic simulation approach implemented in MATLAB software to determine operating conditions based on the locally available solar fraction. The simulation results for the integrated polygeneration and humidification-dehumidification desalination are validated via literature values and THERMOFLEX software. In addition, sensitivity analysis is performed to identify the most influential decision variables on the system performance. These are then defined as objective functions to be optimized via the multi-objective optimization strategy. The latter combines Genetic Programming and Artificial Neural Networks to minimize total costs, environmental impacts, and economic and environmental emergy rates whilst maximizing the desalination unit's exergy efficiency and freshwater production. To do so, three and four-objective optimizations are conducted for the integrated solar-assisted polygeneration and CO$_2$ capture system, and six-objective optimization is performed for the desalination unit. Finally, comprehensive energy, exergy, exergoeconomic, exergoenvironmental, emergoeconomic, and emergoenvironmental (6E) analyses are applied to further investigate the system's thermodynamic, economic, and environmental performances. The integrated solar-assisted polygeneration and CO$_2$ capture system is particularly developed for meeting a greenhouse's power, freshwater, and CO$_2$ demands. Nevertheless, the proposed system and multi-objective methodology can be easily adapted to other low-scale buildings and large-scale industrial applications.

Results from sensitivity analysis reveal that the most significant parameters on the system performance are the pinch temperature of the organic Rankine heat exchanger 1, pinch temperature of the evaporator, solar fraction, superheater outlet temperature, and the isentropic efficiency of the steam turbine 1. The implementation of the three-objective optimization of the integrated polygeneration system reduces total costs, environmental impacts, and total monthly environmental emergy rate by 11.4%, 34.31% and 6.38%, respectively. However, the four-objective optimization of the proposed integrated system further reduces the total costs, environmental impacts, and total monthly environmental emergy rate by 56.81%, 50.19% and 77.07%, respectively. The six-objective optimization of the desalination unit shows that the exergy efficiency is enhanced by 7.3%. Moreover, the total costs, environmental impacts, total monthly economic and environmental emergy rates of the humidification-dehumidification unit are reduced by 36%, 40%, 36.6% and 40%, respectively.

According to the exergy analysis results, the combustion chamber presents the highest amount of exergy destruction compared to the other components (56%), followed by the CO$_2$ capture (10%) and heat recovery steam generator (8%). This analysis also shows that the desalination unit operates efficiently, while the gas turbine cycle exhibits the highest fuel exergy flow and the most exergy destruction compared to the remaining integrated power cycles. Furthermore, results from 6E analyses based on the four-objective optimization indicate that the combustion chamber has the highest amount of exergy destruction compared to the other system components, followed by the CO$_2$ capture unit and the heat recovery steam generator. Therefore, the combustion chamber and CO$_2$ capture unit are the system components which requires improvements from exergoeconomic, exergoenvironmental, emergoeconomic, and emergoenvironmental aspects. As pointed out by the previous results, the proposed machine learning-based multi-objective optimization methodology represents a valuable tool to support decision-makers in implementing more cost-effective and environment-friendly solar-assisted integrated polygeneration systems. Future research will be focused on the:

i. Evaluation of the use of other renewable energy resources such as wind, geothermal, biomass, among others.
ii. Integration of heat storage systems, including hydrogen storage systems.
iii. Application of risk and reliability methods to assess the risks and technical capacity of equipment units.
iv. Application of advanced exergy analysis on the supply cycle to determine the amount of avoidable irreversibility of each system component and the irreversibility caused by the negative effects of other equipment.
v. Use of a heat engine instead of a gas turbine due to its higher efficiency and lower fuel consumption.
vi. More accurate calculation of mass and heat transfer coefficients of the humidification and dehumidification unit in the laboratory unit.
vii. Use of the greenhouse biomass in gasification to produce hydrogen, heating, and power.

Data availability

Data will be made available upon request.

CRediT authorship contribution statement

Nastaran Khani: Investigation, Data curation, Formal analysis, Visualization, Software, Writing – original draft. **Mohammad H. Khoshgoftar Manesh:** Conceptualization, Methodology, Supervision, Writing – review & editing. **Viviani C. Onishi:** Methodology, Formal analysis, Visualization, Writing – review & editing.

Declaration of Competing Interest

The authors declare that they have no known competing financial interests or personal relationships that could have appeared to influence the work reported in this paper.

Data availability

Data will be made available on request.

Appendix A. Further data and mathematical formulation for the system design and optimization

Table A2

Thermodynamic modelling equations, input parameters and unknown variables for the different system components.

22

Equipment Unit	Modelling Equations	Input Parameters	Variables
AC [3]	$W_{AC} = \dot{m}_{air}(T_{ac,out}Cp_{ac,out} - T_1Cp_1)W_{AC} = W_{GT} - W_{net}r_{p,AC} = P_{ac,out}/P_1\eta_{AC} = (r_{p,AC}^{\frac{\gamma_{air}-1}{\gamma_{air}}} - 1)/(T_{ac,out}/T_1 - 1)$	$T_0 = 15°C$ $P_0 = 1.013bar T_1 = T_0 P_1 = P_0 P_{ac,out} = 6.921bar \dot{m}_{air} = 2.973\ kg/s$ $W_{net} = 497.3\ kW$	$W_{AC}\eta_{AC}r_{p,AC}T_{ac,out}$
CC [3]	$\dot{m}_{air}h_{ac,out} + \dot{m}_{fuel}LHV_{fuel}\eta_{CC} - \dot{m}_{fg}h_2 = 0\dot{m}_{air} + \dot{m}_{fuel} - \dot{m}_{fg} = 0P_{cc,out} = P_{ac,out}(1 - \Delta P_{CC})$	$LHV_{fuel} = 50047kJ/kg T_f, P_f TIT = 887.2°C \Delta P_{CC} = 0.04bar \dot{m}_{fuel} = 0.0435kg/s$	$P_{cc,out}\dot{m}_{fg}Q_{cc}\eta_{CC}$
CO$_2$ capture [3]	$\dot{m}_{CO2,in} = \frac{x_{CO2}M_{CO2}}{x_{CO2}M_{CO2} + x_{O2}M_{O2} + x_{H2O}M_{H2O} + x_{N2}M_{N2}} \times m_{fg}\dot{m}_{CO2,out} = \eta_{CO2Capture}\dot{m}_{CO2,in}T_{41} = T_{sat@P_{41}}T_{31} = T_{32} + \Delta T_{Cw}Q_{in,CO2Capture} = 4.028024024057373 \times (\eta_{CO2Capture} \times 100 - 0.00178987160251154)EL_{CO2Capture} = 46.9926801139968 + 0.492473855348899 \times \eta_{CO2Capture} \times 100W_{CO2Capture} = 0.438814557877626 \times (\eta_{CO2Capture} \times 100 - 0.000179238981772301)$	$T_8 = T_{stack}P_8 = P_0 T_{16} = T_{11}P_{16} = P_{11} = P_{41}T_{32}, P_{32}\Delta T_{cw}T_{33},$ $P_{33}\eta_{CO2Capture} = 90\%$	$\dot{m}_{CO2,in}\dot{m}_{CO2,out}T_{41}T_{22}Q_{in,CO2Capture}EL_{CO2Capture}W_{CO2Capture}$
Cond 1 [3]	$\dot{m}_{ORC,1}(h_{21} - h_{20}) + \dot{m}_{cw}(h_{23} - h_{24}) = 0Q_{cond,1} = \dot{m}_{ORC,1}(h_{21} - h_{20})T_{24} = T_{23} + \Delta T_{CW}P_{24} = P_{23} - \Delta P_{cond}P_{20} = P_{21}T_{20} = T_{sat@P_{20}}h_{20} = h_{@P_{20},T_{20}}, h_{23} = h_{water@T_{23},P_{23}}$	$T_{23}, P_{23}\Delta T_{CW}$	$Q_{cond,1}\dot{m}_{cw}T_{24}, P_{24}T_{20}, P_{20}$
Cond 2 [3]	$\dot{m}_{ORC,2}(h_{19} - h_{26}) + \dot{m}_{cw}(h_{29} - h_{30}) = 0Q_{cond,2} = \dot{m}_{ORC,2}(h_{27} - h_{26})T_{30} = T_{29} + \Delta T_{CW}P_{30} = P_{29} - \Delta P_{cond}P_{26} = P_{27}T_{26} = T_{sat@P_{26}}h_{26} = h_{@P_{26},T_{26}}, h_{29} = h_{water@T_{39},P_{39}}$	$T_{29}, P_{29}\Delta T_{CW}$	$Q_{cond,2}\dot{m}_{cw}T_{26}, P_{26}T_{30}, P_{30}$
Dehumidifier [44]	$dL_d = Gd\omega_dGC_{Pg,d}dT_{g,d} = h_g a(T_{g,d} - T_{i,d})L_dC_{PL,d}dT_{L,d} = (h_{L,d}a + C_{PL,d}dL_d)(T_{i,d} - T_{L,d})Gd\omega_{g,d} = k_{g,d}a(\omega_{g,d} - \omega_{i,d})GC_{Pg,d}dT_{g,d} + C_{PL,d}dT_{L,d}L_d + G(C_{Pv}(T_{g,d} - T_0) - C_{PL,d}(T_{L,d} - T_0) + \lambda_0)d\omega_d\omega_i = 2.19 \times 10^{-6}T_i^3 - 1.85 \times 10^{-4}T_i^2 + 7.06\times 10^{-2}T_i - 0.077$	$L_{d,in}G$ $h_g a$ $k_{g,d}\lambda_0 \omega_{in,d}T_{g,h}$	$L_dT_{g,d}T_{L,d}T_{i,d}\omega_{g,d}\omega_{i,d}$
ECO [3]	$\dot{m}_{fg}(h_6 - h_5) + \dot{m}_s(h_{11} - h_{10}) = 0P_6 = P_5 - \Delta P_{ECO,fg}P_{11} = P_{10} - \Delta P_{ECO,s}T_{10} = T_{sat@P_{20}}Q_{ECO} = \dot{m}_s(h_{11} - h_{10})$	$T_{10}, P_{10}\Delta P_{ECO,fg}\Delta P_{ECO,s}T_{11}$	$Q_{ECO}T_6, P_6 P_{11}$
EVA [3]	$\dot{m}_{fg}(h_5 - h_4) + \dot{m}_s(h_{12} - h_{11}) = 0P_5 = P_4 - \Delta P_{EVA,fg}P_{12} = P_{11} - \Delta P_{EVA,s}Q_{EVA} = \dot{m}_{hp}(h_{28} - h_{22})$	$T_4, P_4\Delta P_{EVA,fg}\Delta P_{EVA,s}T_{11}, P_{11}$	$Q_{EVA}T_5, P_5 P_{12}$
GT [3]	$W_{GT} = \dot{m}_{fg}(h_{cc,out} - h_3)P_{23} = P_0 + \sum \Delta P_{HRSG,fg}r_{p,GT} = P_{cc,out}/P_3$ $\eta_{GT} = (1 - T_3/T_{cc,out})/(1 - r_{p,GT}^{\frac{1-\gamma_{fg}}{\gamma_{fg}}})$	$T_3 = TET = 519.8°C$	$W_{GT}P_3r_{p,GT}\eta_{GT}$
Humidifier [44]	$dL_h = Gd\omega_hGC_{Pg,h}dT_{g,h} = h_g a(T_{i,h} - T_{g,h})L_hC_{PL,h}dT_{L,h} = (h_{L,h}a + C_{PL,h}dL_h)(T_{L,h} - T_{i,h})Gd\omega_{g,h} = k_{g,h}a(\omega_{i,h} - \omega_{g,h})GC_{Pg,h}dT_{g,h} + C_{PL,h}dT_{L,h}L_h + G(C_{Pv}(T_{g,h} - T_0) - C_{PL,h}(T_{L,h} - T_0) + \lambda_0)d\omega_h\omega_i = 2.19 \times 10^{-6}T_i^3 - 1.85 \times 10^{-4}T_i^2 + 7.06\times 10^{-2}T_i - 0.077$	$L_{h,in}G$ h_g a $k_{g,h}\lambda_0 \omega_{in,h}T_{L,h,in}T_{g,h,in}$	$L_hT_{g,h}T_{L,h}T_{i,h}\omega_{g,h}\omega_{i,h}$
HPP [3]	$v_9 = v_{sat@P_9}h_{10} = h_9 + v_9 \times (P_{10} - P_9)W_P = \dot{m}_s(h_{10} - h_9)T_{10} = T_{@P_{10},h_{10}}h_{10,is} = h_{@P_{10},s_{10,is}}\eta_P = (h_{10,is} - h_9)/(h_{10} - h_9)$	$P_{10} = P_{pump,out}$	$T_{10}W_P\eta_P$
HX 1 [3]	$P_7 = P_6 - \Delta P_{HX1,s}Q_{HX,1} = \dot{m}_s(h_6 - h_7)P_{22} = P_{19} - \Delta P_{HX1,ORC}$	$T_7T_{22}T_6\Delta P_{HX1,s}\Delta P_{HX1,ORC}P_6$	$Q_{HX,1}P_7P_{22}$
HX 2 [3]	$Q_{HX,2} = \dot{m}_s(h_{17} - h_{18})P_{28} = P_{25} - \Delta P_{HX2,ORC}$	$T_{18}T_{28}T_{17}\Delta P_{HX2,s}\Delta P_{HX2,ORC}P_{17}$	$Q_{HX,2}P_{28}$
SUP [3]	$\dot{m}_{fg}(h_4 - h_3) + \dot{m}_s(h_{13} - h_{12}) = 0P_4 = P_3 - \Delta P_{SH,fg}P_{13} = P_{12} - \Delta P_{SH,s}T_{13} = T_{SH,out}Q_{HPSH} = \dot{m}_s(h_{13} - h_{12})h_{13} = h_{water@T_{13},P_{13}}$	$T_3, P_3\Delta P_{SH,fg}\Delta P_{SH,s}T_{SH,out}T_{12}P_{12}\dot{m}_s$	$Q_{HPSH}T_{10}, P_{10}T_{28}, P_{28}$
ST 1 [3]	$\dot{m}_s(h_{13} - h_{14}) - W_{ST,1} = 0h_{14} = h_{13} - \eta_{ST}(h_{13} - h_{14,is})P_{13} = TIP_{ST1}$ $P_{14} = TIP_{ST2}$	$\eta_{ST} = 88\%\dot{m}_s$	$W_{ST1}T_{14}, P_{14}$
ST 2 [3]	$\frac{\dot{m}_s}{2}(h_{15} - h_{17}) - W_{ST,2} = 0h_{17} = h_{15} - \eta_{ST}(h_{15} - h_{17,is})P_{15} = TIP_{ST2}$ $P_{17} = P_{18} \times \Delta P_{HX2,s}$	$\eta_{ST} = 88\%P_{18}\dot{m}_s$	$W_{ST2}T_{17}, P_{17}$
ORCT 1 [3]	$\dot{m}_{ORC,1}(h_{22} - h_{21}) - W_{ORCT,1} = 0h_{22} = h_{21} - \eta_{ST}(h_{21} - h_{22,is})$	$T_{21}, P_{21}\eta_{ORC}$	$W_{ORCT,1}$
ORCT 2 [3]	$\dot{m}_{ORC,1}(h_{28} - h_{27}) - W_{ORCT,2} = 0h_{27} = h_{28} - \eta_{ST}(h_{28} - h_{27,is})$	$T_{27}, P_{27}\eta_{ORC}$	$W_{ORCT,2}$
ORCP 1 [3]	$P_{19} = P_{20} + \Delta P_{ORCpump,1}v_{20} = v_{sat@P_{20}}h_{19} = h_{20} + v_{20} \times (P_{19} - P_{20})W_{ORC,P1} = \dot{m}_{ORC,2}(h_{19} - h_{20})T_{19} = T_{@P_{19},h_{19}}h_{19,is} = h_{@P_{19},s_{19,is}}\eta_{ORCpump,1} = (h_{19,is} - h_{20})/(h_{19} - h_{20})$	$\Delta P_{ORCpump,1}P_{20}$	$P_{19}W_{ORC,P1}T_{19}\eta_{ORCpump,1}\dot{m}_{ORC,1}h_{19}$
ORCP 2 [3]	$P_{25} = P_{26} + \Delta P_{ORCpump,2}v_{26} = v_{sat@P_{26}}h_{25} = h_{26} + v_{26} \times (P_{25} - P_{26})W_{ORC,P2} = \dot{m}_{ORC,2}(h_{25} - h_{26})T_{25} = T_{@P_{25},h_{25}}h_{25,is} = h_{@P_{25},s_{25,is}}\eta_{ORCpump,2} = (h_{25,is} - h_{26})/(h_{25} - h_{26})$	$\Delta P_{ORCpump,2}P_{26}$	$P_{25}W_{ORC,P2}T_{25}\eta_{ORCpump,2}\dot{m}_{ORC,2}h_{25}$
Solar Collectors	$T_{43} = T_{46} + \Delta T_{pinchSFHX}$ $P_{48} = P_{47} + \Delta P_{SFpump}P_{43} = P_{48} - \Delta P_{solarfield}m_{47}C_{p(therminolI)}(T_{43} - T_{47}) = m_{42}(h_{46} - h_{42})$ $[414239]C_{p(therminolI)} = 1.498 + (0.002414)T + (5.9591 \times 10^{-6})T^2 - (2.9879\times 10^{-8})T^3 + (4.4172 \times 10^{-11})T^4 m_{42} = (1 - SF)m_{20}Q_{solar} = A_c.DNIA_c = n_{mirror}.A_{mirror}A_{mirror} = \frac{A_{module}}{7}$ $A_{module} = 12 \times 5.77\ (m^2)$ $Q_u = m_{48}.C_{p(therminolI)}.(T_{out} - T_{in})[42]$ $Q_u = \eta_c.Q_{solar}\eta_c = 0.75 - 0.000045.(T_{in} - T_{am}) - 0.039.\left(\frac{T_{in} - T_{am}}{DNI}\right) - 0.0003.DNI.\left(\frac{T_{in} - T_{am}}{DNI}\right)^2$	$\Delta P_{SFpump}\Delta P_{solarfield}SF$ DNI $T_8 = T_{46}$ $\Delta T_{pinchSFHX}A_{module}n_{mirror}$	$m_{47}P_{48}P_{43}T_{43}A_{mirror}m_{42}A_c$

Table A3
Purchasing cost equations for different system equipment units.

Equipment Unit	Capital Investment Cost (US$)	Ref.
AC	$Z_{AC} = 0.076 + 0.0003 \times \dot{W}_{net} \times 10^6$	[3]
CC	$Z_{CC} = 0.046 + 0.0002 \times \dot{W}_{net} \times 10^6$	[3]
GT	$Z_{GT} = (0.073 + 0.001 \times \dot{W}_{net} - 1.183 \times 10^{-7} \times \dot{W}_{net}^2) \times 10^6$	[3]
ECO	$Z_{ECO} = 6570\left(\frac{\dot{Q}_{ECO}}{\Delta T_{ECO}}\right)^{0.8} + 21276\dot{m}_w + 1184.4\dot{m}_g^{1.2}$	[45]
EVA	$Z_{EVA} = 6570\left(\frac{\dot{Q}_{EVA}}{\Delta T_{EVA}}\right)^{0.8} + 21276\dot{m}_w + 1184.4\dot{m}_g^{1.2}$	[45]
SUP	$Z_{SUP} = 6570\left(\frac{\dot{Q}_{SUP}}{\Delta T_{SUP}}\right)^{0.8} + 21276\dot{m}_w + 1184.4\dot{m}_g^{1.2}$	[45]
HPP	$Z_{Pump} = 3540\left(\dot{W}_{Pump}\right)^{0.7}$	[46]
ST 1	$Z_{ST1} = 2210\left(\dot{W}_{ST1}\right)^{0.7}$	[45]
ST 2	$Z_{ST2} = 2210\left(\dot{W}_{ST2}\right)^{0.7}$	[45]
HX 2	$Z_{HX2} = 1000(A_{HX2})^{0.65}$	[46]
ORCT 2	$Z_{ORCT2} = 4750\left(\dot{W}_{ORCT2}\right)^{0.75}$	[46]
Cond 2	$Z_{Cond2} = 1773\dot{m}_{ORC1}$	[45]
ORCP 2	$Z_{ORCP2} = 200(\dot{W}_{ORCP2})^{0.65}$	[46]
HX 1	$Z_{HX1} = 1000(A_{HX1})^{0.65}$	[46]
ORCT 1	$Z_{ORCT1} = 4750\left(\dot{W}_{ORCT1}\right)^{0.75}$	[46]
Cond 1	$Z_{Cond1} = 1773\dot{m}_{ORC2}$	[45]
ORCP 1	$Z_{ORCP1} = 200(\dot{W}_{ORCP1})^{0.65}$	[46]
CO_2 capture	$Z_{CO2} = 74 \text{ US\$/ton } CO_2$	[47]
Solar field	$Z_{Solar} = 355 \text{ US\$/m}^2 aperture\ area$	[45]
SFHX	$Z_{SFHX} = 12000\left(\frac{A}{100}\right)^{0.6}$	[45]
SFP	$Z_{SFP} = 3540\left(\dot{W}_{SFP}\right)^{0.7}$	[46]
Humidifier	$Z_{humidifier} = 746.749.\left(L_{h,in}\right)^{0.79}.(R_h)^{0.57}.(A_h)^{-0.9924}.(0.022 T_{wb} + 0.39)^{2.447}$ $R_h = T_{35} - T_{36}$ $A_h = T_{35} - T_{wb}$	[40]
Dehumidifier	$Z_{dehumidifier} = 2143(A_{dehumidifier})^{0.514}$	[40]

Table A4
Weight functions used for each component of the polygeneration system.

Equipment Unit	Weight Function (tone)	Ref.
AC	$Weight = 0.01.\dot{W}_{net} + (-120.48/(1.23.\dot{W}_{net} - 1484.59))$	[3]
CC	$Weight = 0.0001 + 0.006.\dot{W}_{net} + (-2.37/(10482.38 - 9.65.\dot{W}_{net}))$	[3]
GT	$Weight = 0.064.\dot{W}_{net} + 1.13e^{-8}(\dot{W}_{net})^3 - 17.49 - 4.54e^{-5}(\dot{W}_{net})^2$	[3]
ECO	$Weight = 4058.55 + 41.13(T_{sub})^2 + 2096.16.log(T_{sub}).\sqrt{(T_{sub})} - 2172.43.T_{sub}$	[3]
EVA	$Weight = 6948.11 - 1109.97.log\Delta T_{pinch.EVA}$	[3]
SUP	$Weight = 3511.49 + 0.88.\Delta T_{approch.SUP}$	[3]
HPP	$Weight = 0.0061\ (\dot{W}_{HPP})^{0.95}$	[18]
ST 1	$Weight = 4.9\ (\dot{W}_{ST1})^{0.73}$	[45]
ST 2	$Weight = 4\ (\dot{W}_{ST2})^{0.73}$	[45]
HX 2	$Weight = 2.14(\dot{Q}_{HX2})^{0.7}$	[45]
ORCT 2	$Weight = 14(\dot{W}_{ORCT2})$	[45]
Cond 2	$Weight = 0.073(\dot{Q}_{Cond2})^{0.099}$	[45]
ORCP 2	$Weight = 31.22(\dot{W}_{ORCP2})$	[3]
HX 1	$Weight = 2.14(\dot{Q}_{HX1})^{0.7}$	[45]
ORCT 1	$Weight = 14(\dot{W}_{ORCT2})$	[3]
Cond 1	$Weight = 0.073(\dot{Q}_{Cond1})^{0.099}$	[45]
ORCP 1	$Weight = 31.22(\dot{W}_{ORCP2})$	[3]
CO_2 capture	$Weight = 10\ (37.27\ \dot{m}_g + 0.1312(\dot{m}_g)^2)$	[3]
Solar Field	$Weight = 148.44 + 5550.52(\dot{m}_{th})$	[3]
SFHX	$Weight = 2.14(\dot{Q}_{SFHX})^{0.7}$	[45]
SFP	$Weight = 0.0061\ (\dot{W}_{HPP})^{0.95}$	[3]
Humidifier	$Weight = 0.0005(6.84.L_{h,in}.X.Y)$	[3]
Dehumidifier	$Weight = 0.0005(6.84.L_{D,in}.X.Y)$	[3]

Appendix B. Validation results obtained for the proposed system

Table B1

Validation results of thermodynamic properties of the solar energy-driven polygeneration system from the developed MATLAB model [3].

$\dot{m}$ (kg/s)				T (°C)				P (bar)			
Stream	THFX	MATLAB	Error (%)	THFX	MATLAB	Error (%)	THFX	MATLAB	Error (%)		
1	2.973	2.973	0	15	15	0	1.013	1.013	0		
AC, out	2.973	2.973	0	267.3	264.4	1.08	6.92	6.92	0		
2	0.043	0.043	0	25	25	0	9.79	9.79	0		
CC, out	3.017	3.017	0	887.2	887.2	0	6.644	6.644	0		
3	3.017	3.017	0	519.8	519.8	0	1.043	1.044	0.001		
4	3.017	3.017	0	455.2	456.4	0.2	1.041	1.041	0		
5	3.017	3.017	0	276.4	276.3	0.04	1.036	1.036	0		
6	3.017	3.017	0	259.7	260.29	0.2	1.034	1.034	0		
7	3.017	3.017	0	227.8	227.8	0	1.013	1.013	0		
8	2.894	2.892	0.06	35	35	0	1.013	1.013	0		
9	0.3178	0.3178	0	15	15	0	1.04	1.04	0		
10	0.3178	0.3178	0	15.17	15.05	0.8	20.4	20.4	0		
11	0.3178	0.3178	0	212.9.	212.9	0	20.2	20.2	0		
12	0.3178	0.3178	0	212.9	212.9	0	20.2	20.2	0		
13	0.3178	0.3178	0	510	510	0	20	20	0		
14	0.3178	0.3178	0	228	227.2	0.3	2	2	0		
15	0.3178	0.3178	0	165.6	163.6	1.2	2	2	0		
16	0.159	0.159	0	165.6	163.6	1.2	2	2	0		
17	0.159	0.159	0	165.6	163.6	1.2	1.034	1.034	0		
18	0.159	0.159	0	80	80	0	1.014	1.014	0		
19	0.454	0.429	5.5	27.63	27.72	0.3	4.08	4.08	0		
20	0.454	0.429	5.5	27.46	27.46	0	1	1	0		
21	0.454	0.429	5.5	74.06	73.92	0.1	1	1	0		
22	0.454	0.429	5.5	108.7	108.7	0	4	4	0		
23	2.287	2.159	5.6	15	15	0	1.013	1.013	0		
24	2.287	2.159	5.6	24.68	24.68	0	0.994	0.994	0		
25	1.708	1.72	0.7	27.61	27.7	0.3	3.512	3.514	0.06		
26	1.708	1.72	0.7	27.46	27.46	0	1	1	0		
27	1.708	1.72	0.7	79.42	79.27	0.2	1	1	0		
28	1.708	1.72	0.7	110.1	110.1	0	3.443	3.444	0.03		
29	8.771	8.825	0.6	24.68	24.68	0	1.573	1.573	0		
30	8.771	8.825	0.6	15	15	0	1.542	1.525	1.1		
31	21.79	21.79	0	25	25	0	2.068	2.068	0		
32	21.79	21.79	0	15	15	0	3.447	3.447	0		
33	0.109	0.112	0.03	35	35	0	151.7	151.7	0		
42	0.254	0.258	1.5	15.17	15.17	0	20.6	20.6	0		
43	0.681	0.659	3.23	45.15	45.18	0.06	1.014	1.014	0		
44	0.681	0.659	3.23	45.16	45.18	0.04	1.137	1.138	0.09		
45	0.681	0.659	3.23	222.9	222.9	0	1.034	1.034	0		
46	0.254	0.258	1.5	212.9	212.9	0	20.2	20.2	0		
47	0.063	0.6	4.76	15.17	15.17	0	20.4	20.6	0.98		
48	0.063	0.6	4.76	212.9	212.9	0	20.2	20.2	0		

Table B2

Validation results of thermodynamic properties of the humidification-dehumidification (HDH) desalination unit from the developed MATLAB model [3].

Stream	$\dot{m}$ (kg/s.m²)					T (°C)		
	Literature	Ref.	MATLAB	Error (%)	Literature [48]	MATLAB	Error (%)	
34	0.49	[48]	0.49	0	55	55	0	
35	0.28	[48]	0.28	0	24.1	24.1	0	
36	0.28	[48]	0.28	0	36	38	5.5	
37	19.7	[40]	20.1	1.5	45	43	4.4	
38	0.28	[48]	0.28	0	34	33.2	2.4	
39	3.612	[49]	3.59	0.4	29.3	26.8	8.4	
40	1	[48]	1	0	20	20	0	

Table B3

Validation results of main decision variables for different system components.

Parameter	MATLAB	THFX	Error (%)
Q_{SUP}	218.1	219.8	0.77
Q_{EVA}	595.4	600.9	0.91
Q_{ECO}	266.8	267.1	0.11
W_{ST1}	179.2	178.2	0.56
W_{ST2}	39.1	38.04	2.78
W_{ORCT1}	9.46	9.91	4.54
W_{ORCT2}	36.98	36.66	0.87
Q_{ORCHX1}	96.82	101.3	4.42
Q_{ORCHX2}	420.9	421.5	0.14
Q_{cond1}	87.5	90.5	3.31
Q_{cond2}	384.3	384.9	0.15
$EL_{CO_2Capture}$	91.3	85.5	6.78
$W_{CO_2Capture}$	39.5	36.3	8.81
$Q_{in,CO2Capture}$	412.2	380	8.47

References

[1] R. Shah, A. Loo, Advancement in Desalination Using Solar Energy.https://www.altenergymag.com/article/2021/02/advancements-in-desalination-using-solar-energy/34562, (2021). https://www.altenergymag.com/article/2021/02/advancements-in-desalination-using-solar-energy/34562.

[2] National Renewable Energy Laboratory (NREL), U.S. http://www.nrel.gov/csp/solarpaces/by country detail.cfm; website accessed on 27/06/2015., (n.d.).

[3] N. Khani, M.H. Khoshgoftar Manesh, V.C. Onishi, 6E analyses of a new solar energy-driven polygeneration system integrating CO2 capture, organic Rankine cycle, and humidification-dehumidification desalination, J. Clean. Prod. 379 (2022), 134478.

[4] Y.N. Dabwan, P. Gang, J. Li, G. Gao, J. Feng, Development and assessment of integrating parabolic trough collectors with gas turbine trigeneration system for producing electricity, chilled water, and freshwater, Energy 162 (2018) 364–379.

[5] R.S. El-Emam, I. Dincer, Development and assessment of a novel solar heliostat-based multigeneration system, Int. J. Hydrogen Energy 43 (5) (2018) 2610–2620.

[6] B. Ghorbani, Z. Javadi, S. Zendehboudi, M. Amidpour, Energy, exergy, and economic analyses of a new integrated system for generation of power and liquid fuels using liquefied natural gas regasification and solar collectors, Energy Convers. Manag. 219 (2020), 112915.

[7] B. Ghorbani, M. Mehrpooya, M. Sadeghzadeh, Process development of a solar-assisted multi-production plant: Power, cooling, and hydrogen, Int. J. Hydrogen Energy 45 (55) (2020) 30056–30079.

[8] A. Mouaky, A. Rachek, Thermodynamic and thermo-economic assessment of a hybrid solar/biomass polygeneration system under the semi-arid climate conditions, Renew. Energy 156 (2020) 14–30.

[9] N. Tukenmez, M. Koc, M. Ozturk, A novel combined biomass and solar energy conversion-based multigeneration system with hydrogen and ammonia generation, Int. J. Hydrogen Energy 46 (30) (2021) 16319–16343.

[10] H. Xu, Y.J. Dai, Parameter analysis and optimization of a two-stage solar assisted heat pump desalination system based on humidification-dehumidification process, Sol. Energy 187 (2019) 185–198.

[11] E. Deniz, S. Çınar, Energy, exergy, economic and environmental (4E) analysis of a solar desalination system with humidification-dehumidification, Energy Convers. Manag. 126 (2016) 12–19.

[12] M.I. Zubair, F.A. Al-Sulaiman, M.A. Antar, S.A. Al-Dini, N.I. Ibrahim, Performance and cost assessment of solar driven humidification dehumidification desalination system, Energy Convers. Manag. 132 (2017) 28–39.

[13] H. Ghiasirad, N. Asgari, R. Khoshbakhti Saray, S. Mirmasoumi, Thermoeconomic assessment of a geothermal based combined cooling, heating, and power system, integrated with a humidification-dehumidification desalination unit and an absorption heat transformer, Energy Convers, Manag. 235 (2021) 113969.

[14] M. Fischedick, J. Roy, Climate Change 2014: Mitigation of Climate Change. Contribution of Working Group III to the Fifth Assessment Report of theIntergovernmental Panel on Climate Change. Intergovernmental Panel onClimate Change., (2014).

[15] G.G. Esquivel Patiño, F. Nápoles Rivera, Global warming potential and net power output analysis of natural gas combined cycle power plants coupled with CO2 capture systems and organic Rankine cycles, J. Clean. Prod. 208 (2019) 11–18.

[16] X. Liu, X. Yang, M. Yu, W. Zhang, Y. Wang, P. Cui, Z. Zhu, Y. Ma, J. Gao, Energy, exergy, economic and environmental (4E) analysis of an integrated process combining CO2 capture and storage, an organic Rankine cycle and an absorption refrigeration cycle, Energy Convers. Manag. 210 (2020) 112738.

[17] C. Botero, M. Finkenrath, M. Bartlett, R. Chu, G. Choi, D. Chinn, Redesign, Optimization, and Economic Evaluation of a Natural Gas Combined Cycle with the Best Integrated Technology CO2 Capture, Energy Procedia 1 (1) (2009) 3835–3842.

[18] M.H. Khoshgoftar Manesh Manesh, P. Firouzi, S. Kabiri, A.M. Blanco-Marigorta,, Evaluation of power and freshwater production based on integrated gas turbine, S-CO2, and ORC cycles with RO desalination unit, Energy Convers. Manag. 228 (2021) 113607.

[19] M.H. Khoshgoftar Manesh, R.S. Ghadikolaei, H.V. Modabber, V.C. Onishi, Integration of a combined cycle power plant with MED-RO desalination based on

conventional and advanced exergy, exergoeconomic, and exergoenvironmental analyses, Processes. 9 (2020) 59.

[20] E. Jadidi, M.H. Khoshgoftar Manesh, M. Delpisheh, V.C. Onishi, Advanced exergy, exergoeconomic, and exergoenvironmental analyses of integrated solar-assisted gasification cycle for producing power and steam from heavy refinery fuels, Energies 14 (24) (2021) 8409.

[21] S. Anvari, O. Mahian, H. Taghavifar, S. Wongwises, U. Desideri, 4E analysis of a modified multigeneration system designed for power, heating/cooling, and water desalination, Appl. Energy 270 (2020), 115107.

[22] M.A. Ehyaei, S. Baloochzadeh, A. Ahmadi, S. Abanades, Energy, exergy, economic, exergoenvironmental, and environmental analyses of a multigeneration system to produce electricity, cooling, potable water, hydrogen and sodium-hypochlorite, Desalination 501 (2021) 114902.

[23] M. Nourpour, M.H. Khoshgoftar Manesh, Modeling and 6E analysis of a novel quadruple combined cycle with turbocompressor gas station, J. Therm. Anal. Calorim. 147 (8) (2022) 5165–5197.

[24] S.A. Makkeh, A. Ahmadi, F. Esmaeilion, M.A. Ehyaei, Energy, exergy and exergoeconomic optimization of a cogeneration system integrated with parabolic trough collector-wind turbine with desalination, J. Clean. Prod. 273 (2020) 123122.

[25] H.R. Abbasi, H. Pourrahmani, Multi-criteria optimization of a renewable hydrogen and freshwater production system using HDH desalination unit and thermoelectric generator, Energy Convers. Manag. 214 (2020) 112903.

[26] Y. Liu, J. Han, H. You, Exergoeconomic analysis and multi-objective optimization of a CCHP system based on LNG cold energy utilization and flue gas waste heat recovery with CO2 capture, Energy 190 (2020) 116201.

[27] M.A. Lozano, A. Valero, Theory of the exergetic cost, Energy 18 (9) (1993) 939–960.

[28] A. Bejan, G. Tsatsaronis, M.J. Moran, Thermal design and optimization, John Wiley & Sons, 1995.

[29] I. Dincer, M.A. Rosen, Exergy: Energy, Environment and Sustainable Development (2020), https://doi.org/10.1016/B978-0-12-824372-5.09986-3.

[30] W.J. Wepfer, R.A. Gaggioli, E.F. Obert, Proper Evaluation of Available Energy For HVAC, ASHRAE Trans, 1979.

[31] G. Tsatsaronis, J. Pisa, Exergoeconomic evaluation and optimization of energy systems - application to the CGAM problem, Energy 19 (3) (1994) 287–321.

[32] A. Lazzaretto, G. Tsatsaronis, SPECO: A systematic and general methodology for calculating efficiencies and costs in thermal systems, Energy 31 (8-9) (2006) 1257–1289.

[33] M. Aghbashlo, M. Tabatabaei, S. Soltanian, H. Ghanavati, A. Dadak, Comprehensive exergoeconomic analysis of a municipal solid waste digestion plant equipped with a biogas genset, Waste Manag. 87 (2019) 485–498.

[34] L. Meyer, G. Tsatsaronis, J. Buchgeister, L. Schebek, Exergoenvironmental analysis for evaluation of the environmental impact of energy conversion systems, Energy 34 (1) (2009) 75–89.

[35] M. Aghbashlo, M.A. Rosen, Consolidating exergoeconomic and exergoenvironmental analyses using the emergy concept for better understanding energy conversion systems, J. Clean. Prod. 172 (2018) 696–708.

[36] F. Yang, H. Cho, H. Zhang, J. Zhang, Y. Wu, Artificial neural network (ANN) based prediction and optimization of an organic Rankine cycle (ORC) for diesel engine waste heat recovery, Energy Convers. Manag. 164 (2018) 15–26.

[37] E.K.P. Chong, An introduction to optimization Edwin K.P. Chong, Stanislaw H. Żak., 2008.

[38] Z. Wang, G.P. Rangaiah, Application and Analysis of Methods for Selecting an Optimal Solution from the Pareto-Optimal Front obtained by Multiobjective Optimization, Ind. Eng. Chem. Res. 56 (2) (2017) 560–574.

[39] H. Yu, H. Helland, X. Yu, T. Gundersen, G. Sin, Optimal design and operation of an Organic Rankine Cycle (ORC) system driven by solar energy with sensible thermal energy storage, Energy Convers. Manag. 244 (2021) 114494.

[40] T. Gholizadeh, M. Vajdi, H. Rostamzadeh, Exergoeconomic optimization of a new trigeneration system driven by biogas for power, cooling, and freshwater production, Energy Convers. Manag. 205 (2020) 112417.

[41] A. Rovira, R. Barbero, M.J. Montes, R. Abbas, F. Varela, Analysis and comparison of Integrated Solar Combined Cycles using parabolic troughs and linear Fresnel reflectors as concentrating systems, Appl. Energy 162 (2016) 990–1000.

[42] Z. Xi, S. Eshaghi, F. Sardari, Energy, exergy, and exergoeconomic analysis of a polygeneration system driven by solar energy with a thermal energy storage tank for power, heating, and freshwater production, J. Energy Storage. 36 (2021) 102429.

[43] E. Lüpfert, E. Zarza, M. Geyer, P. Nava, J. Langenkamp, W. Schiel, A. Esteban, R. Osuna, E. Mandelberg, Euro Trough collector qualification complete-performance test results from PSA, in: ISES Sol. World Congr. 2001 2003 Proc., 2003.

[44] M. Zamen, M. Amidpour, M.R. Firoozjaei, A novel integrated system for fresh water production in greenhouse: Dynamic simulation, Desalination 322 (2013) 52–59.

[45] E.J.C. Cavalcanti, Exergoeconomic and exergoenvironmental analyses of an integrated solar combined cycle system, Renew. Sustain. Energy Rev. 67 (2017) 507–519.

[46] I. Dincer, M.A. Rosen, P. Ahmadi (Eds.), Optimization of Energy Systems, Wiley, 2017.

[47] E.S. Rubin, J.E. Davison, H.J. Herzog, The cost of CO2 capture and storage, Int. J. Greenh. Gas Control. 40 (2015) 378–400.

[48] M. Zamen, M. Amidpour, Modeling of Humidification and Dehumidification Process anddesign of HD desalinator for production of fresh water ingreenhouse and analysis of the combined system, (2013).

[49] A. Eslamimanesh, M.S. Hatamipour, Economical study of a small-scale direct contact humidification-dehumidification desalination plant, Desalination 250 (1) (2010) 203–207.